Received: 8 June 2023 | Revised: 22 April 2024 | Accepted: 11 June 2024

DOI: 10.1111/gbi.12609

gebiology WILEY

ORIGINAL ARTICLE

Primary to post-depositional microbial controls on the stable and clumped isotope record of shoreline sediments at Fayetteville Green Lake

Hanna C. Leapaldt[1] | Carie M. Frantz[2] | Juliana Olsen-Valdez[3] | Kathryn E. Snell[3] | Elizabeth J. Trower[3] | Miquela Ingalls[1]

[1]Department of Geosciences, The Pennsylvania State University, University Park, Pennsylvania, USA

[2]Department of Earth and Environmental Sciences, Weber State University, Ogden, Utah, USA

[3]Department of Geological Sciences, University of Colorado, Boulder, Colorado, USA

Correspondence
Hanna C. Leapaldt and Miquela Ingalls, Department of Geosciences, The Pennsylvania State University, University Park, PA, USA.
Email: hcl5089@psu.edu and ingalls@psu.edu

Funding information
National Science Foundation, Grant/Award Number: 1826850; Geological Society of America; College of Earth and Mineral Sciences, Pennsylvania State University

Abstract

Lacustrine carbonates are a powerful archive of paleoenvironmental information but are susceptible to post-depositional alteration. Microbial metabolisms can drive such alteration by changing carbonate saturation *in situ*, thereby driving dissolution or precipitation. The net impact these microbial processes have on the primary $\delta^{18}O$, $\delta^{13}C$, and Δ_{47} values of lacustrine carbonate is not fully known. We studied the evolution of microbial community structure and the porewater and sediment geochemistry in the upper ~30 cm of sediment from two shoreline sites at Green Lake, Fayetteville, NY over 2 years of seasonal sampling. We linked seasonal and depth-based changes of porewater carbonate chemistry to microbial community composition, in situ carbon cycling (using $\delta^{13}C$ values of carbonate, dissolved inorganic carbon (DIC), and organic matter), and dominant allochems and facies. We interpret that microbial processes are a dominant control on carbon cycling within the sediment, affecting porewater DIC, aqueous carbon chemistry, and carbonate carbon and clumped isotope geochemistry. Across all seasons and sites, microbial organic matter remineralization lowers the $\delta^{13}C$ of the porewater DIC. Elevated carbonate saturation states in the sediment porewaters ($\Omega > 3$) were attributed to microbes from groups capable of sulfate reduction, which were abundant in the sediment below 5 cm depth. The nearshore carbonate sediments at Green Lake are mainly composed of microbialite intraclasts/oncoids, charophytes, larger calcite crystals, and authigenic micrite—each with a different origin. Authigenic micrite is interpreted to have precipitated in situ from the supersaturated porewaters from microbial metabolism. The stable carbon isotope values ($\delta^{13}C_{carb}$) and clumped isotope values (Δ_{47}) of bulk carbonate sediments from the same depth horizons and site varied depending on both the sampling season and the specific location within a site, indicating localized (μm to mm) controls on carbon and clumped isotope values. Our results suggest that biological processes are a dominant control on carbon chemistry within the sedimentary subsurface of the shorelines of Green Lake, from actively forming microbialites to pore space organic matter remineralization and

micrite authigenesis. A combination of biological activity, hydrologic balance, and allochem composition of the sediments set the stable carbon, oxygen, and clumped isotope signals preserved by the Green Lake carbonate sediments.

KEYWORDS
carbonate, clumped isotopes, diagenesis, geomicrobiology, microbialite, sedimentology

1 | INTRODUCTION

Carbonate minerals capture information about their formation environment, and thus can be used to reconstruct ancient climate and tectonics throughout Earth's history. Lacustrine carbonates source their carbon and oxygen from the water in which they form. As such, the carbonate oxygen ($\delta^{18}O_{carb}$) and carbon ($\delta^{13}C_{carb}$) isotope ratios can be related to the oxygen and the dissolved inorganic carbon (DIC) compositions of the formation water via predictable water-mineral fractionation (Coplen, 2007; Emrich et al., 1970; Kim & O'Neil, 1997; Romanek et al., 1992). These values can then be related to the regional and local processes that influence meteoric water and carbon. Lacustrine carbonate sediments, in particular, are used to create regional records of terrestrial paleoclimate and biogeochemical cycles. The lacustrine carbonate record has shaped much of our understanding of the response of terrestrial environments and ecosystems to regional or global stresses (e.g., Dansgaard, 1964; Leng & Marshall, 2004; Li & Ku, 1997; Pietzsch et al., 2020; Rowley, 2007; Steinman & Abbott, 2013; Talbot, 1990; Thompson et al., 1990).

Both the temperature of lake water and the oxygen isotope composition of the lake water ($\delta^{18}O_w$) determine the oxygen isotope values of carbonate forming in the lake water ($\delta^{18}O_{carb}$). The $\delta^{18}O$ value of lake water is affected by elevation and latitude, (which alters $\delta^{18}O$ of precipitation) and relative amount of evaporation. In hydrologically open systems, $\delta^{18}O_{carb}$ can be used to reconstruct $\delta^{18}O$ values of precipitation and ancient elevations (e.g., Currie et al., 2016; Ingalls et al., 2017; Ingalls, Frantz, et al., 2020; Ingalls, Rowley, et al., 2020; Poage & Chamberlain, 2001; Rozanski et al., 1993; Talbot, 1990). In hydrologically closed lakes, lake water $\delta^{18}O_w$ values are typically higher than $\delta^{18}O_w$ values of regional meteoric water due to Rayleigh distillation of lake water during evaporation (Leng & Marshall, 2004). Carbonate minerals that form in equilibrium with lake water thus record the relative ^{18}O-enrichment at the time of mineral formation and can be used to reconstruct evaporation-precipitation balance and paleo-aridity (Dansgaard, 1964; Steinman & Abbott, 2013; Talbot, 1990). $\delta^{13}C_{carb}$ values can be related to basin-scale primary productivity (Leng & Marshall, 2004) as well as past partial pressure and $\delta^{13}C$ values of atmospheric CO_2 (Pietzsch et al., 2020). In closed basin lakes, $\delta^{13}C_{carb}$ and $\delta^{18}O_{carb}$ values are often positively correlated, with both trending towards higher values with increasing evaporation (Li & Ku, 1997).

These traditional interpretations require an assumption that the stable isotope values of lacustrine carbonates are controlled solely by hydroclimate and water column processes and remain unaltered after deposition. However, complex biogeochemical cycles that occur at both the basin scale and shorter length scales contribute to lacustrine carbonate geochemistry and isotopic signatures. For example, when microorganisms metabolize, they cycle nutrients and major ions (e.g., C, N, P, and S species) that impact carbonate chemistry. Microbial metabolisms mediate the components of aqueous chemistry that set the carbonate saturation state of a given carbonate mineral, Ω, by producing or consuming dissolved inorganic carbon (DIC) and/or alkalinity (ALK; a measure of a solution's ability to buffer the addition of protons). The saturation state (Ω) of calcium carbonate is defined as $\Omega = \frac{\alpha_{Ca^{2+}} * \alpha_{CO_3^{2-}}}{K_{sp}}$, where $\alpha_{Ca^{2+}}$ and $\alpha_{CO_3^{2-}}$ are the activities of Ca^{2+} and CO_3^{2-} in solution, and K_{sp} is the solubility product constant for a given carbonate polymorph at the temperature, pressure, and salinity of the solution (Zeebe & Wolf-Gladrow, 2001). Because microbial metabolisms can alter both DIC and alkalinity concentrations, which in turn can impact the CO_3^{2-} concentration, microbial metabolisms can result in changes to Ω. Ultimately, the magnitude of change in Ω can be predicted based on the ratio of net change in alkalinity to net change in DIC concentration ($\Delta ALK/\Delta DIC$) caused by the metabolism's net reaction (Bergmann et al., 2013). Because the carbonate saturation state governs whether a solution favors carbonate mineral dissolution ($\Omega < 1$) or precipitation ($\Omega > 1$), microbial activity is an important lever in carbonate mineralization and alteration in the sediment porewater. In addition to altering Ω, different microbial metabolisms result in unique carbon isotope fractionations within lake and sediment porewaters due to distinct carbon fixation pathways. As a result, authigenic microbial carbonate precipitating from sediment porewaters may have distinct $\delta^{13}C_{carb}$ values (Blättler et al., 2015; Claypool & Kaplan, 1974; Ingalls, Frantz, et al., 2020; Meister et al., 2007). Microbial subsurface processes are also hypothesized to impact carbonate clumped isotope values (Δ_{47}; the relative abundance of the $^{13}C^{18}O^{16}O$ isotopologue; Ingalls, Frantz, et al., 2020; Ingalls, Rowley, et al., 2020; Petryshyn et al., 2015; Thaler et al., 2020). In other words, isotopic measurements of bulk carbonate that include a mass fraction of authigenic carbonate (i.e., carbonate that precipitated from sediment porewaters) may not reflect basin-scale processes alone. Here, we connect processes occurring in the lacustrine sediment subsurface – both microbiological and physicochemical – to the isotopic signatures ($\delta^{18}O_{carb}$, $\delta^{13}C_{carb}$, and Δ_{47}) of bulk lacustrine carbonate sediment.

We measured $\delta^{13}C_{carb}$ and $\delta^{18}O_{carb}$ of shoreline carbonate sediments, stable carbon isotope ratios of the porewater ($\delta^{13}C_{DIC}$) and organic matter ($\delta^{13}C_{org}$), and the major ion concentrations of the porewater at two shoreline sites in Green Lake, NY, USA to evaluate

the geochemistry at different depths in the sediment over 2 years. The core locations were within the well-mixed, upper, oxic portion of the lake. We used 16S rRNA gene amplicon sequencing to identify the microbial clades present at each depth and to ultimately connect the microbial community in the sediments with porewater and sediment geochemistry. We identified the allochems present within the sediment to understand the paragenesis of shoreline carbonate sediment at Green Lake. We identified proto-facies present in the shallow sediments to diagnose which carbonate facies may be most affected by microbial processes. We also measured Δ_{47} values of a subset of carbonate samples to determine how microbial carbon cycling impacts the clumped isotope temperatures preserved by the sediments. In doing so, we determined the impacts of microbial carbon cycling on driving early diagenesis and on what signals are preserved in the lacustrine carbonate record of Green Lake with the goal of informing isotope-based interpretations of the lacustrine rock record—especially of shoreline microbial carbonate facies.

1.1 | Geologic setting and carbonate geobiology of Fayetteville Green Lake

Green Lake in Fayetteville, New York is well-studied due to a redox structure thought to be comparable to Proterozoic oceans (Havig et al., 2018), and the known influence of microbes in both water column whiting precipitation and active microbialite bioherms lining the steep margined shorelines. Green Lake is a closed-basin, meromictic lake, with a chemocline that permanently separates the oxic upper layer (mixolimnion) from the anoxic bottom layer (monimolimnion; Thompson et al., 1990). This results in a redox gradient from lake surface to bottom, and a dense bacterial layer between mixolimnion and monomolimnion. Both Green Lake and its neighboring (upstream) Round Lake are primarily recharged by saline, sulfate-rich groundwater that percolates through the evaporite-rich (i.e., gypsum ($CaSO_4 \bullet H_2O$), dolomite ($CaMg(CO_3)_2$), and halite-rich (NaCl)) Syracuse and Vernon Shale Formations of the Silurian Salina Group (Thompson et al., 1990). The permanent stratification is attributed to the density contrast between the saline bottom layer and decreased wind stress due to the steep-basin geometry of the lake (Thompson et al., 1990). The permanent redox stratification and sulfur-rich incoming groundwater have a major influence on the lake's microbial community structure: photosynthesis and aerobic respiration are the main metabolisms in the mixolimnion, while paired sulfate reduction and sulfide oxidation are the main metabolisms at the chemocline, and anaerobic oxidation of organic matter and methanogenesis are the main metabolisms below the chemocline (Thompson et al., 1990). Green Lake has been used to understand carbon cycling and fluxes in ancient redox-stratified and euxinic environments, like intermittent periods of the late Paleoproterozoic and Mesoproterozoic ocean (Havig et al., 2018; Meyer & Kump, 2008), despite the fact that sulfate concentrations were likely much lower in the Proterozoic ocean than in the modern (e.g., Chu et al., 2007; Gellatly & Lyons, 2005).

Microbial photosynthesis drives carbonate precipitation in multiple ways in Green Lake. Previous work has demonstrated the biogenicity of "whiting events" at Green Lake, a phenomenon that occurs in some shallow marine and lacustrine environments today (Stanton et al., 2022; Thompson et al., 1997). These studies have shown that water column calcite precipitation during whiting events in the lake is controlled by photosynthetic cyanobacteria (*Synechococcus*) and diatoms and relies on extracellular polymeric substances (EPS) to scaffold mineralization (Kamennaya et al., 2020; Stanton et al., 2022). Photosynthetic cyanobacteria also induce carbonate precipitation on the surface of the thrombolitic bioherms in Green Lake, which are clotted microbialites that line the east and northwest shores of Green Lake (DeMott et al., 2020; Thompson & Ferris, 1990; Wilhelm & Hewson, 2012).

2 | METHODS

2.1 | Field sampling

Sediment cores, porewater samples, and lake water samples were collected from Green Lake every fall, spring, and summer from September 2020 to July 2022 (Table S2). Each season, at least one sediment core and suite of water samples were taken at a location on the eastern shore of the lake (Bioherm East; BHE) in the reworked sediments on top of a thrombolite bioherm (Figure 1a–c). BHE cores did not penetrate the thrombolite underneath the reworked sediment. In the summer 2021 and spring 2022, a sediment core and water samples were also collected at a location on the southern shore of the lake at the inlet from Round Lake to Green Lake (Round Lake Inflow South; RIS; Figure 1a). Sediment cores were taken at approximately 40 cm water depth at both locations. During each sampling session and at each site, surface water, ambient air temperature, and lake water pH were measured. Additionally, a HOBO Pendant® MX Temperature/Light Data Logger was deployed in fall 2020 at the BHE location and collected data every 30 min from September 19, 2020 to April 10, 2021 (Figure S1). In spring 2022, porewater temperatures were measured using a k-type temperature probe connected to a multimeter. The temperature probe was attached to a metal rod and inserted into the sediment at 5 cm depth increments.

During all site visits, the upper ~30 cm of sediments were extracted via push coring with PVC core liners. One core (known as the "long core" collected from BHE in spring 2022, denoted as Spring 2022b) was collected using a slide hammer corer. All sample types described herein were collected at 5 cm depth increments. In the field, porewater was extracted through 0.15 μm pore size rhizons (Rhizosphere) connected to 10 mL syringes inserted into holes drilled at 5 cm depth increments downcore (Figure 1d). Details of how porewater was treated in the field for DIC, pH, and ion analyses can be found in the Data S1.

After collecting the porewater, the core was sliced into 5 cm intervals while being extruded from the core liner such that sample

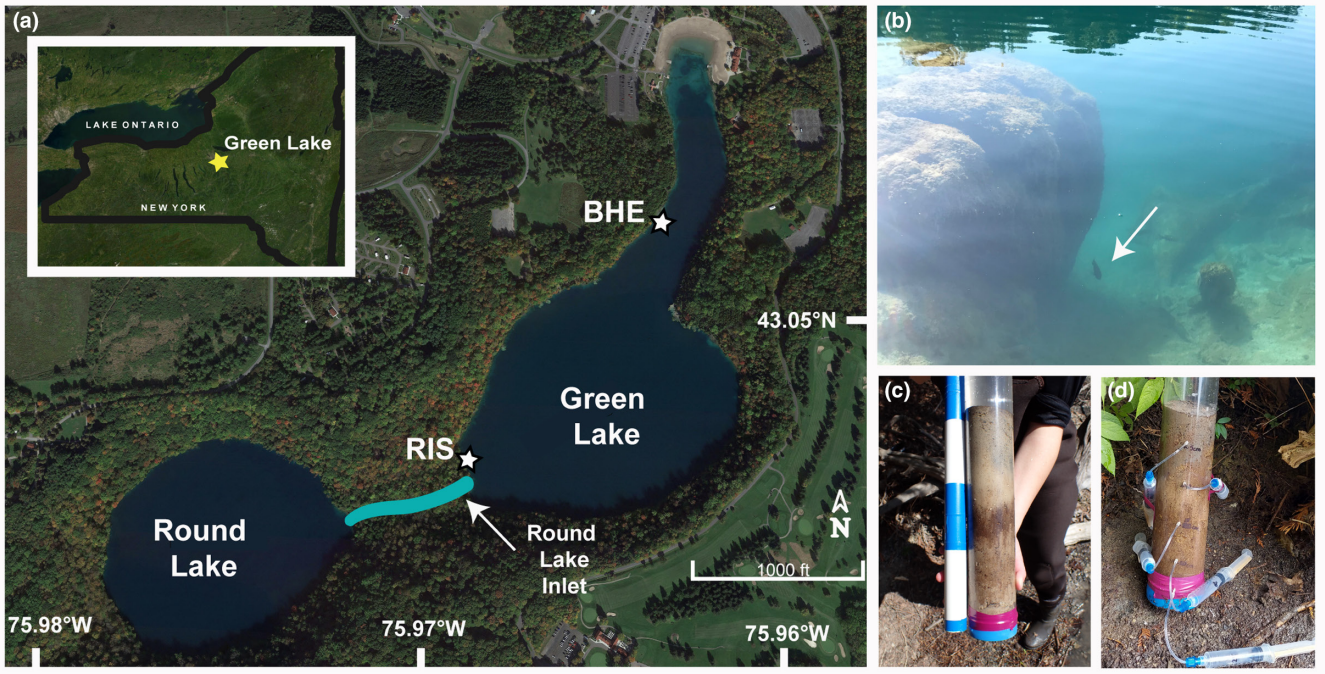

FIGURE 1 (a) Location of Green Lake and sampling sites Bioherm East (BHE) and Round Lake Inflow South (RIS) on the Green Lake shoreline (base map courtesy of Google Earth). (b) A thrombolite bioherm at BHE (white arrow pointing to ~20 cm fish for scale; pictured bioherm is approximately 1 m across). (c) Example of a push core taken during the April 2021 sampling season. Blue and white intervals are each 10 cm. (d) Example setup of core porewater extraction with rhizons and syringes.

"5 cm" represents sediment from 0 to 5 cm depth, "10 cm" is sediment from 5 to 10 cm depth, and so on. From each section, bulk sediment was collected in polypropylene conical centrifuge tubes for carbonate stable isotope and facies analyses, and into glass vials for organic matter isotope analyses. Excluding the summer 2022 samples, sediment from each section was also collected for DNA extraction using an acetone-sterilized spatula into 2 mL lysis tubes prefilled with Zymo Research bashing beads and 750 μL of DNA/RNA Shield, as well as surface waters collected using a sterile syringe. All samples were frozen on dry ice in the field and stored in a −20°C freezer at Penn State until further processing.

2.2 | Sample treatment

Details of sediment pre-treatment protocols for organic carbon and carbonate isotope analyses can be found in the Data S1.

2.2.1 | DNA extractions and sequencing

DNA was extracted from the samples using a Zymo Research Quick-DNA Fecal/Soil Microbe DNA Miniprep kit. A ThermoScientific Nanodrop was used to quantify nucleic acid concentrations in the samples. Once extracted and quality checked, samples were sent to Wright Lab (Huntingdon, PA) where they were amplified, primed, and sequenced for the 16S rRNA gene following the Earth Microbiome Project protocol (Thompson et al., 2017; Walters et al., 2015). DNA was amplified using the 515f/806r primer pair to amplify the 16S V4 region, with Illumina adapters on the 5′ and 3′ ends (515F: Parada et al., 2016: 806R: Apprill et al., 2015). Wright Lab sequenced the samples using Illumina MiSeq v2 chemistry with paired-end 250 base pair reads.

2.3 | Measurements

2.3.1 | Stable isotope measurements

All isotopic values are reported in permille (‰) relative to the VPDB standard (i.e., $\delta^{13}C = [(^{13}C/^{12}C)_{sample}/(^{13}C/^{12}C)_{VPDB}] \times 1000$). For each stable isotope measurement, corrections were made for linearity, instrumental drift, and offsets from standards, and major outliers were culled. Instrument details, standardization, and determination of measurement accuracy and precision for each measurement can be found in the Data S1.

2.3.2 | Carbonate clumped isotope measurements and temperature calculations

Carbonate clumped isotopes values, Δ_{47}, are defined by $\Delta_{47} = \left(\frac{R^{47}}{R^{47*}} - 1\right) \times 1000$ where $R^{47} = (2[^{13}C^{18}O^{16}O] + 2*[^{12}C^{17}O^{18}O] + [^{13}C^{17}O_2])/[^{12}C^{16}O_2]$ for the sample, and R^{47*} is that ratio given a stochastic distribution of the heavy isotopes for the same bulk isotopic composition. The temperature dependence of a given Δ_{47}

value is such that the preferential "clumping" of the heavier isotopes of oxygen (^{18}O) and carbon (^{13}C) occurs at colder temperatures, and decreases with progressively warmer temperatures (Eiler, 2007). The Δ_{47} measurements of the Green Lake carbonate sediment samples were made on a Thermo 253 Plus with a Protium Isotopologue Batch EXtractor (IBEX) at Penn State. Details of the digestion and CO_2 gas purification within the IBEX can be found in the Data S1.

Δ_{47} values were obtained for depths of 5, 15, and 25 cm for cores from the 2020 to 2021 sampling year and depths of 35, 40, and 50 from the "long core" (spring 2022b) in spring 2022. Each sample Δ_{47} value had ≥3 replicates, where each replicate had ≥8 acquisitions and each acquisition had 10 cycles. Temperatures for each sample were calculated using the T-Δ_{47} calibration of Anderson et al. (2021). Error from both analytical uncertainties and standardization were propagated through to the final $\Delta_{47,I\text{-}CDES}$ values using the Python package "D47crunch" (Daëron, 2021).

2.3.3 | Porewater and lake water ion measurements

Cation concentrations were measured on a Thermo iCAP 7400 Inductively Coupled Plasma-Atomic Emission Spectroscopy (ICP-AES; Na^+, K^+, Ca^{2+}, Li^+, Mg^{2+}, and Si^{4+}), and anion concentrations were measured on a Dionex™ ICS-2100 Integrated IC System (IC; Cl^-, SO_4^{2-}) at the Penn State Laboratory for Isotopes and Metals in the Environment (LIME). Samples were diluted for the ICP-AES (Table S3) but not for the IC. A calibration curve was created from a suite of High Purity Standards. An EPA 200.7 standard with known concentrations of the ions measured was measured over a range of concentrations on both the ICP-AES and the IC as a quality check to ensure the accuracy of measurements. Accuracy was better than ±0.12 ppm across all measurements. Reported measurements were in μg/mL and were converted to mM.

2.3.4 | Sedimentology

Samples from fall 2020, summer 2021, and spring 2022 were rinsed with DI water and air-dried. Loose sediments were sent to Spectrum Petrographics, Inc. (fall 2020 and summer 2021) and Wagner Petrographic (spring 2022) to create thin sections. Images of the thin sections were taken using a Zeiss AxioScan and AxioImager at PSU. Thin section analysis was used to identify dominant grain types and fabrics in each site and sample. We point-counted the grain types found at three depths (5, 15, and 25/30 cm) at both sites using JMicrovision (Roduit, 2022). We counted ≥400 grains per thin section to quantify the contribution of each grain type to our bulk isotopic analyses. By 400 grains counted, the proportion (in percent) of each grain category stabilized and did not change with additional grains counted for each sample. The proto-lithology was assigned using Dunham classifications under the assumption that the sediments would become lithified as-is to predict which facies would be found in the rock record for each sediment type. Select samples were analyzed using X-ray diffraction (XRD) to confirm calcite is the main mineralogical phase of the samples (details of analysis in Data S1 section 1.7; Figure S2).

2.4 | Calculations and data treatment

2.4.1 | Calcite saturation state

We used the R package "phreeqc" using the Pitzer database to model the saturation index (SI) of calcite, with dissolved ion concentrations, [DIC], temperature, and pH of the Green Lake porewater samples as inputs. Ω was calculated from SI where $\Omega = 10^{SI}$. PHREEQC was also used to calculate $[CO_3^{2-}]$ from this data (Figure S7).

2.4.2 | Processing pipeline of raw 16S rRNA sequences

A QIIME 2 pipeline was used for sequence processing and analysis (Bolyen et al., 2019). Sequences of samples from cores collected in September 2020, April 2021, and July 2021 (Year 1 samples) were filtered together in a batch, and sequences from September 2021, May 2022, and July 2022 (Year 2 samples) were filtered together in a second batch, then all samples were pooled to assign taxonomy. Amplicon sequence variants (ASVs) classified as mitochondria or chloroplast were filtered from the dataset. Demultiplexed sequences were then trimmed at position 220 in the forward read and 190 in the reverse for Year 1 samples, and 190 in the forward and reverse for Year 2. All sequences were denoised, paired ends joined, error-checked, and dereplicated. Chimeric sequences were screened for and removed using the consensus method using DADA2 (Callahan et al., 2016). Singleton sequences were removed. The SILVA 138.1 SSU NR 99 reference database of sequences was used to assign taxonomy to ASVs (Quast et al., 2013; Yilmaz et al., 2014). The database was first prepped for QIIME import using RESCRIPt (Robeson II et al., 2021), during which reference sequences were quality controlled and culled using default settings and read lengths below 900 bp (Archaea) or 1200 bp (Bacteria) were removed. Reads were extracted between the 515f/806r primer pair used for sample amplification, dereplicated, and then used to train a naïve Bayesian taxonomy classifier (Pedregosa et al., 2011), which was used to assign taxonomy to our ASVs. Eight contaminant sequences were identified based on their abundance in most samples and extraction blanks and were removed (Table S5). Four samples (0920-FGL-20-3, 0920-FGL-10-1, 0522-FGL-5-b, and 0522-LC-30 cm-A) that were substantially different in composition and sequence count from replicates were removed from downstream analyses. MAFFT was used to align sequences (Katoh et al., 2002). Rarefaction plots were generated to determine an appropriate sampling depth for diversity analyses in QIIME: samples with less than 3114 sequences were excluded from diversity analyses. This included eight samples all of which had replicates with greater sequence counts, besides the

lake water sample from RIS summer 2021. All sequence FASTQ files used for this study were deposited to the public National Center for Biotechnology Information (NCBI) Sequence Read Archive (SRA) database under BioProject PRJNA916981 BioSample accession numbers SAMN35677971–SAMN35678027.

3 | RESULTS

3.1 | Sedimentology and facies

3.1.1 | Bioherm East (BHE)

All cores at BHE exhibited a light tan color in the upper 10 cm and transitioned to become visibly darker in color between 10 and 15 cm in the core. The dominant allochems identified in the BHE sediments were grains 100–500 μm in size, identified as either microbialite intraclasts or in situ formed oncoids (Figure 2d,e). Both likely have a microbial origin, but formed in different locations. Determining whether these grains are intraclasts or oncoids required diagnosing a genetic origin, addressed in the discussion. These grains were made up of (1) 5–50 μm, subhedral to euhedral calcite crystals that were translucent in plane polarized light and arranged in shrubby (Figure 2f) or radial (Figure 2i) fabrics, and (2) low porosity, clotted carbonate mud (which we use interchangeably with micrite, to mean a grain size less than <4 μm; Figure 2d,e). Clotted carbonate mud is expressed as dark, typically rounded, masses of carbonate with spaces in between that can be filled with crystalline carbonate. The intraclasts/oncoids made up ≥61.5% of the sediment at BHE in the fall 2020 core. The proportion of shrubby calcite to clotted micrite fabric within the grains decreased with depth, and by 25 cm depth, the micritic fabric made up 70% of the internal fabric of these grains. Other allochems within the BHE sediment included 5–50 μm calcite crystals, micrite, and charophyte thalli fragments (calcifying algae; mainly in sediment below 10 cm depth, Figure 2c). In addition to carbonate grains, organic matter was a significant component of the sediment but decreased in abundance with depth (Figure 3). Organic matter fragments were commonly found in spatial association with micrite (Figures S3 and S4). BHE sediments were classified as proto-packstone in the Dunham scheme (Figure 2a,b).

3.1.2 | Round Lake Inlet South (RIS)

RIS cores had a greyish, organic-rich upper 10 cm that transitioned to a light tan color below 10 cm. At RIS, the dominant allochems identified were carbonate mud and charophytes. The charophyte grains were composed of a mixture of 1–10 μm anhedral calcite crystals and micrite (Figure 4e–g). Some charophyte grains had excess carbonate precipitation, and some were partially dissolved into fragments of the original grain as evidenced by wall-thinning (Figure S5). Intraclasts made up of charophyte fragments, and other organic matter fragments, and cemented by micrite were found throughout the RIS sediment and were up to ~1000 μm in size (Figure 4d). The abundance of the intraclasts and charophyte fragments decreased with depth, and the micrite increased with depth (Figure 3). The proto-facies for the RIS sediment were classified as wackestone to packstone (Figure 4a,b).

3.2 | Water chemistry and geochemistry

Green Lake water temperatures at our sites ranged from 10.4 to 25.4°C across all seasons. Porewater temperatures, which were measured spring and summer 2022, ranged from 14 to 23°C, and decreased from the temperature of the overlying water column with depth in sediment by ~3°C by 25 cm sediment depth (Figure 5). The water and geochemical results were described separately for Year 1 (includes cores/samples from fall 2020, spring 2021, and summer 2021) and Year 2 (includes cores/samples from fall 2021, spring 2022, and summer 2022; Tables S3 and S4).

3.2.1 | Dissolved ions concentrations

Ca^{2+} was the most abundant cation in both the porewater and the surface water, ranging from 2.01 to 9.60 mM in porewater and 2.29 to 10.41 mM in the surface water across all depths and seasons. Cation concentrations (Ca^{2+}, Na^{+}, Mg^{2+}, and K^{+}) generally decreased from the sediment–water interface to 20 ± 5 cm depth (Figure S6). Dissolved silica increased in the first 5–10 cm, then decreased with depth. Since we did not find diatoms in the sediment, but they are known to be present in the water column (Stanton et al., 2022), we interpret that this is likely due to diatom frustule dissolution in the upper 10 cm. Sulfate was the most abundant anion, with concentrations ranging from 1.07 to 8.45 mM in the porewater and 2.62 to 9.88 mM in the surface water across all depths and seasons. Like most cations, across all seasons, [SO_4^{2-}] decreased from the sediment–water interface to a minimum at around 20 cm below which [SO_4^{2-}] increased with depth (Figure S6). Chloride concentration ranged from 0.21 to 0.98 mM in the porewaters and on average decreased with depth (Figure S6).

3.2.2 | DIC concentrations

DIC concentrations ranged from 0.83 to 7.26 mmol/kgw in the porewaters and 0.65 to 5.34 mmol/kgw in the surface water across all seasons and depths (Table S3). [DIC] was greatest in the lake water in spring 2021 and in the porewater in summer 2021 at the BHE location. The minimum [DIC] occurred in fall 2020 for both the porewater and lake water. On average for all cores/seasons, [DIC] increased with depth until around ~20 cm, below which [DIC] decreased.

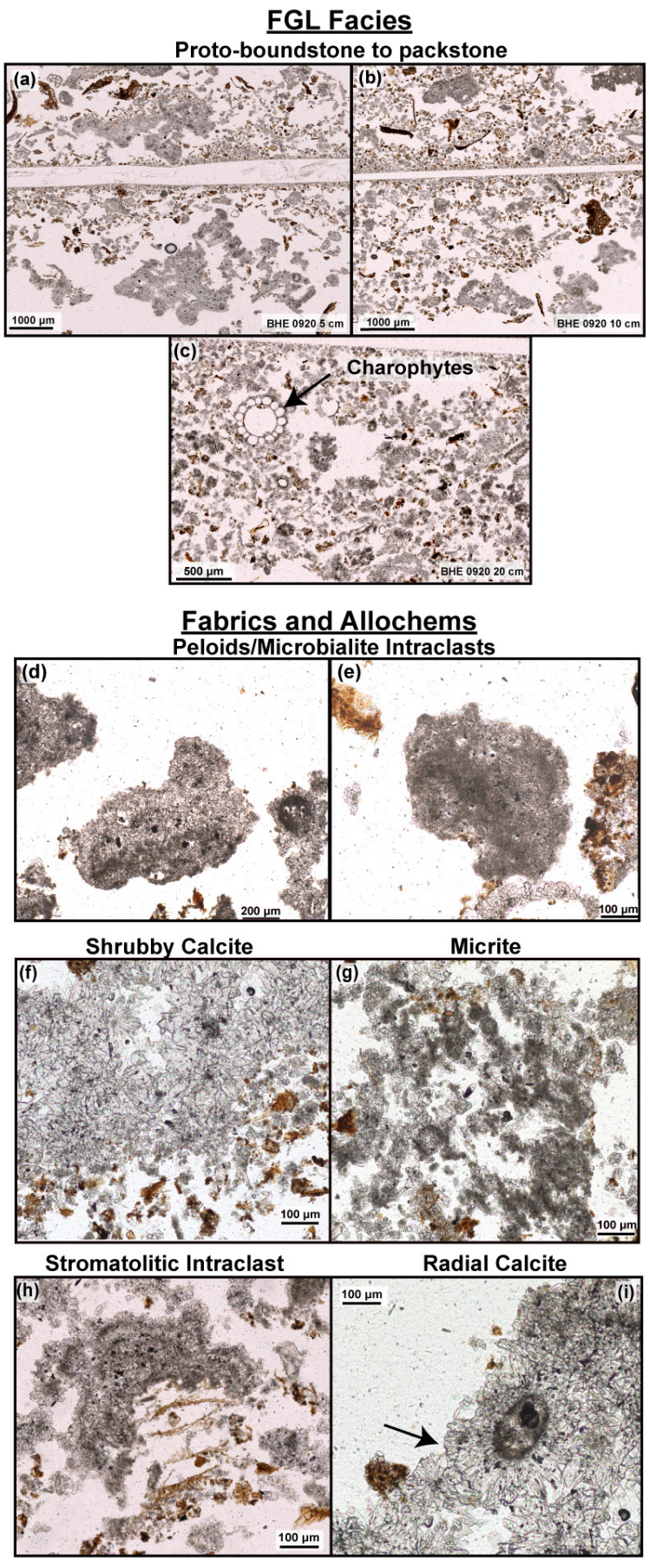

FIGURE 2 Plane-polarized transmitted light microscopy photographs of sediments at Green Lake showing the dominant proto-facies (a–c) and grain types (d–i) at Bioherm East (BHE) from fall 2020 sediments. Arrow in (i) denoting approximately 80 µm subhedral calcite crystals radiating from organic core. Note that the near-horizontal transparent region in (a, b) is an artifact of thin section preparation.

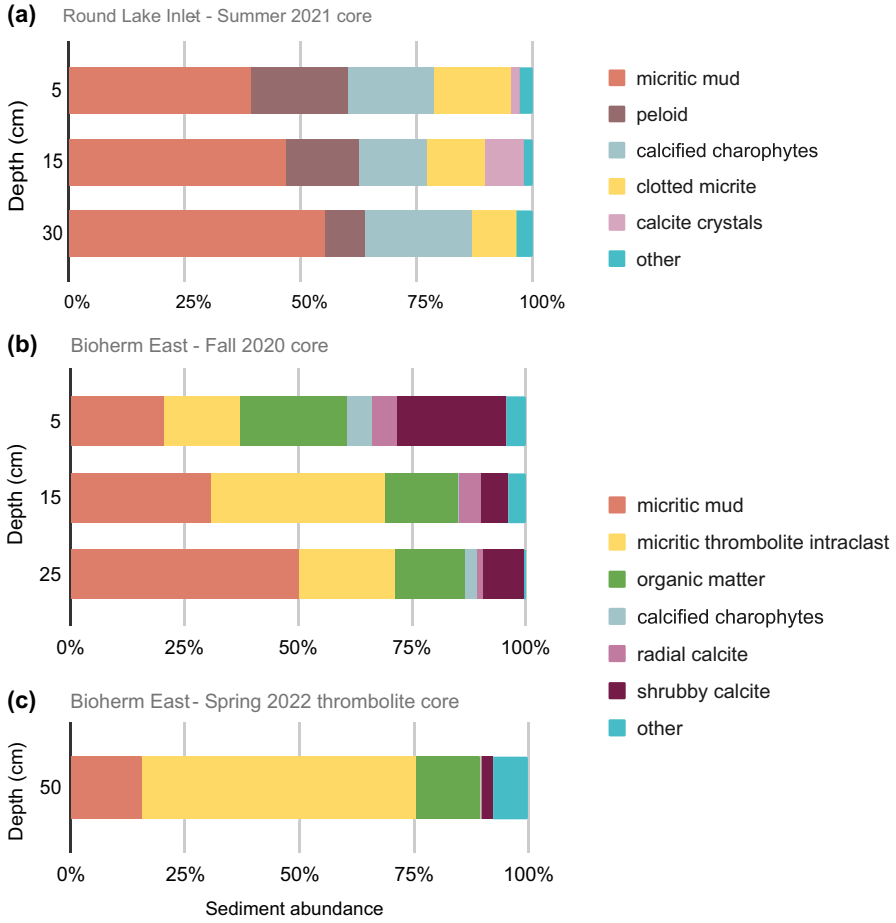

FIGURE 3 Abundances of major grain types found at Round Lake Inflow South (RIS) (a) and Bioherm East (BHE) (b, c), and how they change with depth.

3.2.3 | Calcite mineral saturation state

Calcite is the dominant carbonate mineral precipitating in the photic zone at Green Lake (Thompson et al., 1990). Across all sites and depths, calcite saturation state (Ω_{cal}) was above mineral saturation ($\Omega_{cal}>1$) in both the lake water and porewater in all Year 1 cores (Figure 6), and for one of the Year 2 cores. Ω_{cal} values ranged from 1.82 to 8.69 in the porewater in Year 1, and 0.32 to 16.20 in Year 2. At BHE, porewater Ω_{cal} values reached a maximum value in fall 2021 at 5 cm depth and minimum in the spring 2022 at 20 cm depth. The lake water Ω_{cal} values at BHE were 2.70, 14.38, and 5.46 in fall, spring, and summer for Year 1 and 4.47, 1.38, and 4.34 in fall, spring, and summer for Year 2. The RIS lake water Ω_{cal} value was 2.15 in summer 2021 and 3.08 in spring 2022. The RIS porewater maximum Ω_{cal} value occurred at 25 cm depth and minimum Ω_{cal} value at 35 cm depth. On average, porewater Ω_{cal} values decreased with depth until ~25 cm. At either 25 cm or 30 cm, seven out of the nine cores show an increase in porewater Ω_{cal} values (Figure 6; Table S3).

3.2.4 | Organic carbon isotopes

Across all sites and seasons, $\delta^{13}C_{org}$ values ranged from −26.4 to −31.7‰ VPDB, a range typical for C3 plant-derived organic matter (Kohn, 2010). On average at BHE, $\delta^{13}C_{org}$ values decreased slightly with depth, whereas at RIS $\delta^{13}C_{org}$ values increased with depth (Figure S8), but these trends between depth and $\delta^{13}C_{org}$ were not strongly correlated ($R^2<0.3$).

3.2.5 | DIC carbon isotopes

Surface water $\delta^{13}C_{DIC}$ values ranged from −8.7 to −6.8‰VPDB across all sites and seasons. Porewater $\delta^{13}C_{DIC}$ values ranged from −10.2 to −15.2‰ at BHE and −14.6 to −19.5‰ at RIS (Figure 6). For all cores, $\delta^{13}C_{DIC}$ values decrease by an average of 6.2‰ between the shallow lake water or sediment–water interface DIC and the uppermost 5 cm of sediments. The $\delta^{13}C_{DIC}$ values increased with depth after reaching a minimum; however, the depth of this inflection point varied from 10 to 25 cm depending on the season and site (Figure 6).

3.2.6 | Carbonate carbon and oxygen isotopes

The $\delta^{18}O_{carb}$ values across both years ranged −10.5 to −7.1‰ VPDB among all seasons and depths in sediment at BHE (Figures 7 and S9). The $\delta^{13}C_{carb}$values at BHE across both years range from −3.9 to −1.2‰ VPDB (Figures 7 and S9). The $\delta^{13}C_{carb}$ values at the same depth horizons are up to 2.2‰ different depending on the season the core was taken, despite the BHE core being extracted from

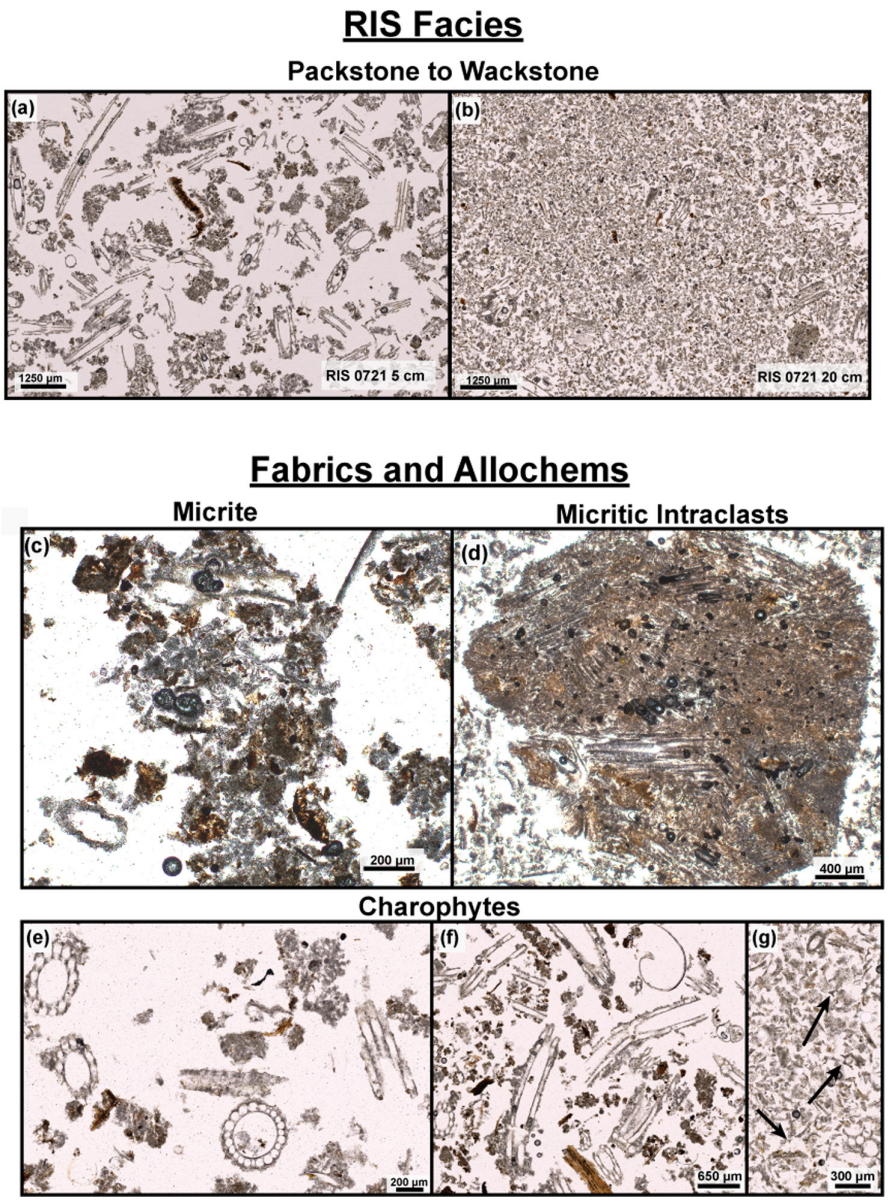

FIGURE 4 Plane-polarized transmitted light microscopy photographs of sediments at Green Lake showing the dominant proto-facies (a, b) and grain types (c–g) at RIS from summer 2021 sediments. Arrows in panel (g) denote triangular calcified charophyte fragments common throughout the RIS sediment.

approximately the same shoreline location atop the same bioherm shelf with less than a meter between each core location in different seasons (Figure 6). The $\delta^{13}C_{carb}$ patterns with depth in the sediment differed depending on season. In Year 1, fall and spring core $\delta^{13}C_{carb}$ values decreased in the first 10 cm depth in sediment, then increased until between 20 and 25 cm depth (Figure 6). In contrast, in the Year 1 summer samples, the $\delta^{13}C_{carb}$ values increased for the first 15 cm depth in sediment but had no discernable pattern below 15 cm (Figure 6). In Year 2 samples, the down core trends were variable, even between cores taken on the same day, only 1 m apart (spring 2022a and spring 2022b; Figure 6). For both Year 1 and Year 2 cores, there was the most variability in $\delta^{13}C_{carb}$ values between cores at the 5 cm depth and the lowest variability at the 25 cm depth (Figure 6).

The RIS $\delta^{18}O_{carb}$ values were, on average, lower than at BHE, ranging from −11.1 to −8.9‰ VPDB (Figures 7 and S9) The $\delta^{13}C_{carb}$ values from RIS samples ranged from −3.51 to −1.2‰ VPDB (Figure 7). In both the Years 1 and 2 RIS cores, $\delta^{13}C_{carb}$ values increased until 15 cm depth, below which there was no distinct pattern (Figure 7). Notably, the most similar downcore trends in $\delta^{13}C_{carb}$ values occur in the summer 2021 RIS core, summer 2021 BHE core, and the spring 2022 RIS core, rather than between the two cores taken at the same site and same season (spring 2022a BHE and spring 2022b BHE; Figure 6).

3.2.7 | Carbonate clumped isotopes

The average Δ_{47} values for the community-accepted standards, ETH2, ETH3, ETH4, and IAEA-C2 (used to create the empirical transfer function (Data S1 section 1.6; Figures S10–S14, Table S1)) during the two analytical periods were 0.209 ± 0.038, 0.613 ± 0.026, 0.451 ± 0.030, and 0.646 ± 0.026 (±2σ). The uncertainties on the empirical transfer function for each analytical session are reported in the Data S1.

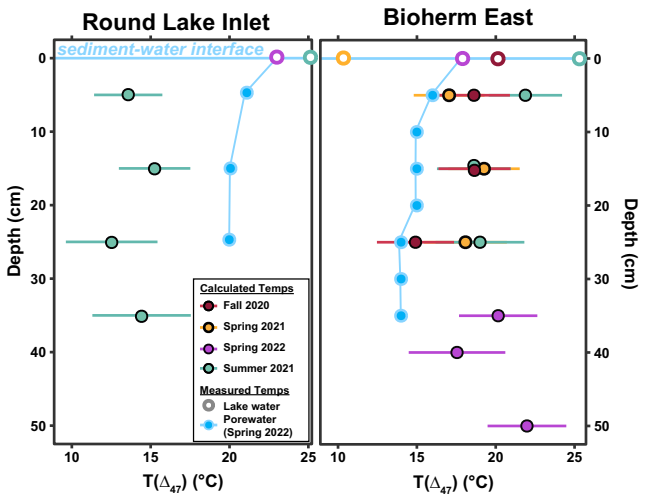

FIGURE 5 Temperatures calculated from carbonate clumped isotope values for cores fall 2020, spring 2021, and summer 2021 (both locations) from Year 1 for depths 5, 15, 25, and 35 (RIS only) cm below sediment–water interface, and depths 35, 40 and 50 cm from the spring 2022 long core. Error bars are calculated from the minimum and maximum Δ_{47} based on standard error. A standard error of Δ_{47} represents the fully propagated allogenic and autogenic standard errors calculated using ClumpyCrunch (Daëron, 2021). Lake water temperatures at the time of core extraction are plotted as open circles. A porewater temperature profile (blue) was measured in May 2022 for comparison to T(Δ_{47}).

The $\Delta_{47,I\text{-}CDES,90}$ values for all samples measured ranged from 0.603 ± 0.007 (±σ) to 0.633 ± 0.01‰ yielding a temperature range of 12.5 ± 2.9 to 22.0 ± 2.5°C (Figure 5). The range of clumped isotope values obtained across each season at BHE was 0.603 ± 0.007 to 0.618 ± 0.007 at 5 cm depth, 0.611 ± 0.007 to 0.613 ± 0.007 at 15 cm, and 0.615 ± 0.008 to 0.625 ± 0.008 at 25 cm. The smaller range of measured Δ_{47} values at 15 cm led to a smaller range in calculated temperatures at 15 cm than for 5 and 25 cm depths (Figure 5). The average clumped isotope-derived temperature recorded by the uppermost 5 cm of sediment is 17.4°C but ranges between 13.3 and 21.5°C. The average T(Δ_{47}) decreases to an average of 15.8°C by 25 cm depth.

3.2.8 | 16S rRNA gene sequencing

In the surface water, the dominant phylum across all seasons was Actinobacteria, a phylum of mainly organoheterotrophs that commonly participate in lignin decay (Eisenlord & Zak, 2010), followed by various orders of Gammaproteobacteria (Figure 8). In the RIS lake water, however, the dominant family was Bathyarchaeia, known for sulfate reduction (Zhou et al., 2018). Cyanobacteria made up a small portion of sequenced bacteria in the lake water samples despite being known to be widespread in the surface waters of Green Lake. Underrepresentation of cyanobacteria in 16S rRNA gene sequencing has been observed in other work, and the low abundance of cyanobacteria detected in our 16S rRNA gene sequencing results for

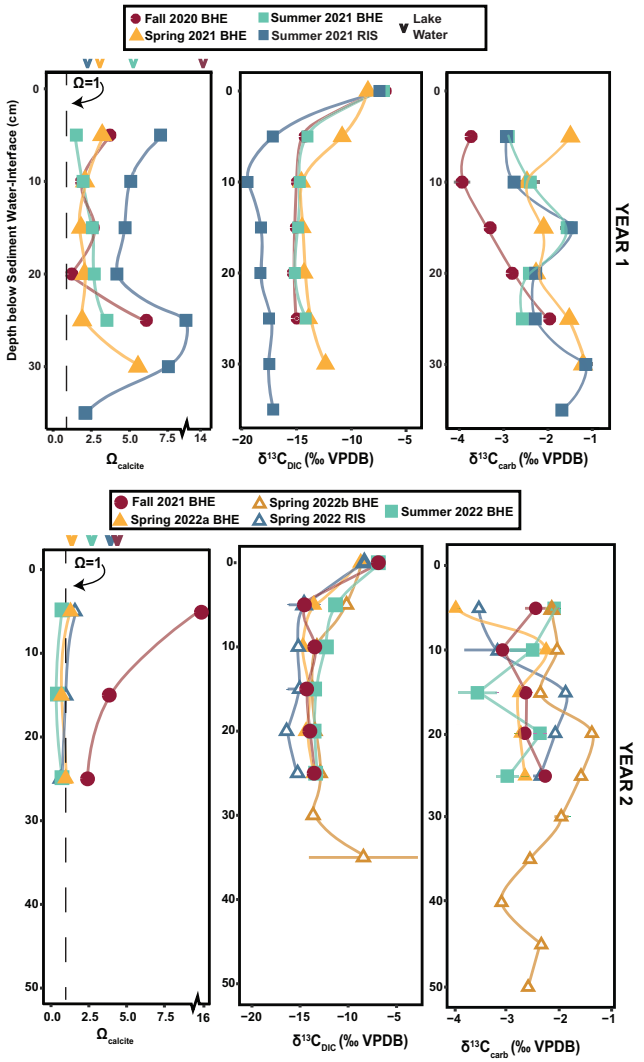

FIGURE 6 Depth profiles for calcite saturation state (Ω), $\delta^{13}C_{DIC}$, and $\delta^{13}C_{carb}$ for all cores in Years 1 (upper) and 2 (lower), and lake water (carets). Error bars represent the standard deviations of individual measurements for $\delta^{13}C_{DIC}$ and $\delta^{13}C_{carb}$. Note that axis breaks for Year 1 and 2 $\Omega_{calcite}$ represent different changes to the x-axis.

both the surface water and sediment–water interface may be due to ineffective lysing of cyanobacteria because of protective EPS (Águila et al., 2021; Frantz et al., 2023; Garcia-Pichel et al., 2001).

The three most diverse samples were all from 5 cm depth (BHE 0421 5 cm, BHE 0721 5 cm, and RIS 0522 5 cm; Figure S15 and S16). Gammaproteobacteria, made up of families like Comamonadaceae (many of which are capable of aerobic respiration (Willems, 2014)), was the dominant class in the 5 cm samples. Below 5 cm depth, the majority of samples decreased in alpha diversity (Figures 8, S15 and S16). Below 5 cm, Bathyarchaeia became most abundant at BHE and the candidate phylum Sva0485 at RIS, both of which have members able to reduce sulfate (Concheri et al., 2017; Vuillemin et al., 2018; Zhou et al., 2018). Across all seasons and sites, various other sulfur cyclers are common (e.g., Thermodesulfovibrionia and Desulfobaccia; Henry et al., 1994).

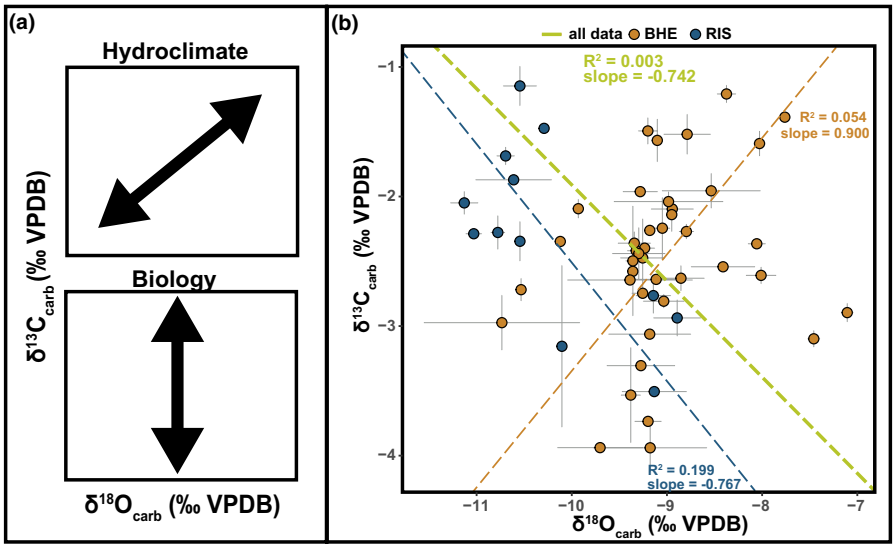

FIGURE 7 (a) Hypotheses demonstrating expected covariance between $\delta^{13}C_{carb}$ and $\delta^{18}O_{carb}$ when water column hydrologic balance processes are being preserved by the stable isotope values and the lack of covariance expected between $\delta^{13}C_{carb}$ and $\delta^{18}O_{carb}$ when *in situ* microbial carbon cycling is instead being recorded. (b) $\delta^{13}C_{carb}$ versus $\delta^{18}O_{carb}$ for all samples, separated by location. The R package "smatr" was used to perform the linear standardized major axis regression (SMA) to generate the lines and to obtain the squared correlation coefficients for data set (Warton et al., 2012). Error bars represent standard deviations of replicate analyses.

4 | DISCUSSION

4.1 | Carbonate $\delta^{13}C$ and $\delta^{18}O$ lack expected correlation for closed basin lakes

Green Lake is considered hydrologically closed, yet the sediment lacked the typical $\delta^{13}C_{carb}$–$\delta^{18}O_{carb}$ positive correlation expected of a closed basin lake ($R^2 < 0.3$; Figure 7). The BHE sediment $\delta^{13}C_{carb}$ versus $\delta^{18}O_{carb}$ values have a slight and statistically insignificant positive correlation ($R^2 = 0.054$), so $\delta^{13}C_{carb}$ and $\delta^{18}O_{carb}$ are considered uncorrelated (Figure 7b). $\delta^{13}C_{carb}$ and $\delta^{18}O_{carb}$ values of RIS sediments yield a weak negative correlation ($R^2 = 0.199$; Figure 7b). When evaluating all Green Lake carbonate samples together, there is no statistically significant correlation between $\delta^{18}O_{carb}$ and $\delta^{13}C_{carb}$ values ($R^2 = 0.003$ and a negative slope). These trends require an alternative explanation for the main control on the carbonate stable isotope values. A large range in both $\delta^{13}C_{carb}$ and $\delta^{18}O_{carb}$ contributes to the lack of correlation. However, the range in $\delta^{18}O_{carb}$ is likely explained by the hydrologic differences between BHE and RIS: the RIS sampling location is near a stream inlet, and therefore has lower $\delta^{18}O_{carb}$ values, whereas sediments at BHE source their oxygen from the well-mixed, evaporatively ^{18}O-enriched epilimnion (Figure S9). Similar $\delta^{18}O_{carb}$ values in the surface sediment of the two sites may reflect a recent decrease in the contribution of the stream at RIS. Nonetheless, the difference in $\delta^{18}O_{carb}$ among cores taken at the same site and same depth is, on average, <0.5‰. In contrast, the range in $\delta^{13}C_{carb}$, especially when considering carbonate from the same site and same depth horizons, needs further explanation. We combined sedimentological evidence with microbial community and geochemical data to show that both hyperlocal (1) spatial heterogeneity and (2) in situ carbonate precipitation and dissolution help explain the lack of covariation and range in $\delta^{13}C_{carb}$ values within the Green Lake shoreline sediments.

4.1.1 | Allochems record different processes and diagenetic histories

The unique formation and/or diagenetic mechanisms of the various allochems in Green Lake sediment may impart specific isotopic signatures that could affect the bulk carbonate values (Figures 2 and 4). The most abundant grain category at BHE, the thrombolite intraclasts/oncoids, are made of a combination of micrite and shrubby calcite. Some grains in this category exhibit preserved laminations (Figure 3h), but most have no laminations. The grains in this category are either transported from the nearby thrombolite (thrombolite intraclast) or formed in situ from localized microbial carbon cycling (oncoid). Some of these grains have similar textures to samples collected directly from the exterior surfaces of the thrombolite bioherms in Green Lake (Figure 2d,e; DeMott et al., 2020), but most of the grains lack lamination observed on the thrombolite exterior (Figure S17). Many of the clotted structures formed on and/or around organic matter on a micro- and macroscopic scale (Figures S3 and S4). An organic matter "nucleus" suggests that some of these grains were instead oncoids that may have formed from photosynthesis at the sediment-water interface, microbial remineralization of other organic carbon during burial (e.g., detrital leaves or fecal matter), or a combination of both. Furthermore, the relative ratio of micritic fabric to shrubby calcite fabric within these grains increased with depth while organic matter decreased (Figure 3). This could have resulted from the contribution of anaerobic metabolisms consuming organic matter below 5 cm depth in the sediment,

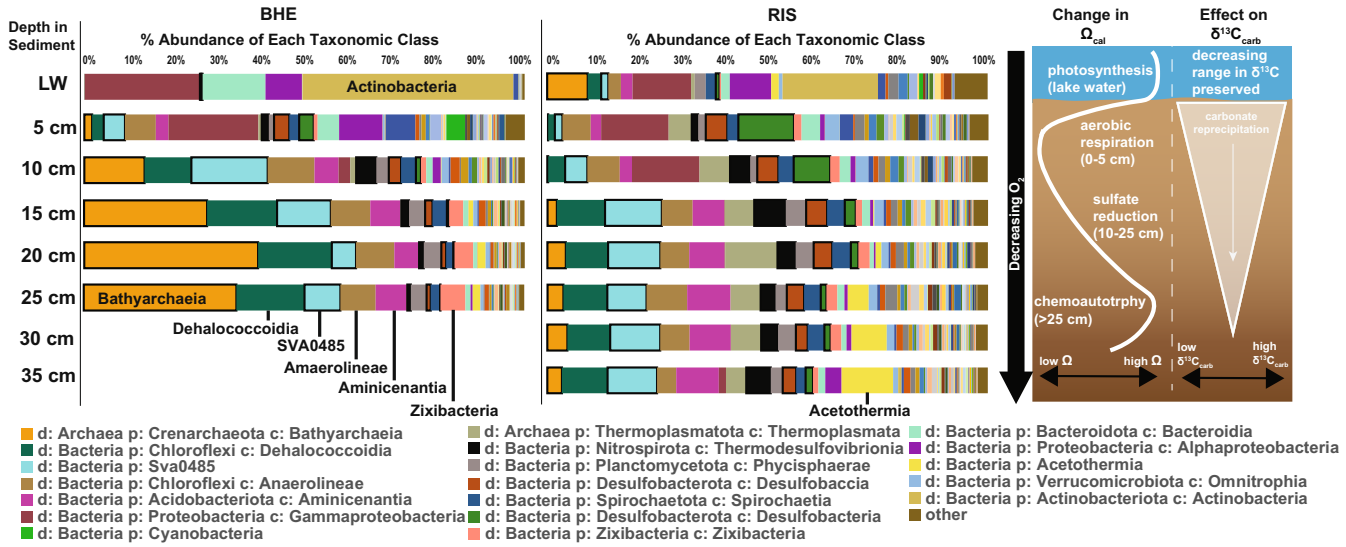

FIGURE 8 Predicted change in calcite saturation state and effect on $\delta^{13}C_{carb}$ based on the dominant microbial classes present at each depth and inferred dominant metabolism. % abundance of each microbial class is shown for summer 2021 cores from Bioherm East (BHE) and Round Lake Inflow South (RIS). Colors for the most abundant 20 classes are shown in the key. Taxa with known ability for sulfur cycling metabolisms are outlined in black. Information for 16S gene sequencing results for all samples in the OSF.

some of which increase Ω and can cause precipitation of carbonate mud (Figure 9).

The contribution of the oncoid/thrombolite intraclast grain category to the bulk $\delta^{13}C_{carb}$ of may be a mixture of both heavier and lighter values. Previous measurements of thrombolites at Green Lake have found $\delta^{13}C$ values that are enriched ~3–4‰ relative to the water column because of photosynthetic impacts on the local DIC pool (Thompson et al., 1997). However, the abundance of clotted micrite preferentially growing on woody and other organic substrates within the sediment suggests that carbonate forming from isotopically lighter DIC in the pore spaces, due to microbial organic matter remineralization, may also make up a fraction of these grains. Since both photosynthesis and forms of anaerobic heterotrophy may contribute to the carbonate formation in these grains, clotted micrite likely records a combination of photic zone, nearshore, and sediment subsurface processes in their $\delta^{13}C_{carb}$ values.

Micrite (Figures 2g and 4c) separate from the intraclasts and oncoids was a dominant component at both sites and the most abundant grain category at RIS. We interpret this grain type as authigenic carbonate that precipitated *in situ* due to carbonate saturation states elevated by microbial metabolism and availability of abundant EPS for $CaCO_3$ nucleation. Authigenic carbonate that precipitates from sediment porewater preserves $\delta^{13}C_{carb}$ values of porewater composition that are isotopically distinct (^{13}C-depleted) from the water column (Section 4.2; Figure 6). Authigenic carbonate precipitation may respond to seasonally and spatially variable Ω in the porewaters (Figure 6) and could provide one mechanism for the observed seasonal and spatial variation in $\delta^{13}C_{carb}$ at the same depth horizons.

Authigenic micrite is a known secondary phase in lacustrine carbonate sediments (Freytet & Verrecchia, 2002), but its contribution to the isotopic signatures of the bulk lacustrine carbonate record

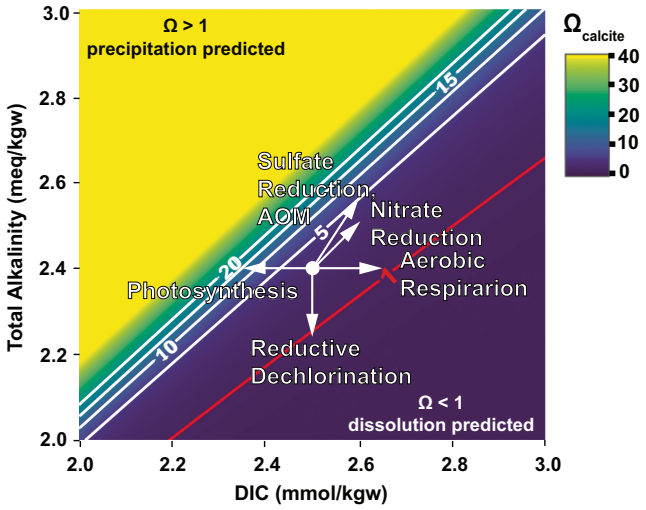

FIGURE 9 Fan diagram representing estimated relative changes in calcite saturation state in response to different microbial metabolisms. The arrows are based on the relative change in alkalinity to change in DIC ($\Delta ALK/\Delta DIC$) estimated for given metabolism and stoichiometry of organic molecule consumed or produced, based on stoichiometric assumptions in Bergmann et al. (2013). Contours of calcite mineral saturation state are specific to the ionic chemistry of Green Lake water. The vertex of the vectors was chosen as an average representative of the porewater of Green Lake. AOM stands for anaerobic oxidation of methane.

is less studied. Recent work from Lake Van (Turkey) revealed water column aragonite and low-Mg calcite co-occur with diagenetic, pore space-precipitated aragonite (McCormack & Kwiecien, 2021). They found the pore space and early diagenetic aragonite to have $\delta^{13}C_{carb}$

values distinct from primary carbonate fabrics. At Kiritimati Lake, on the central Pacific Island Republic of Kiribati, micritic carbonate sediment that was interpreted to have formed in association with heterotrophic metabolisms in the subsurface had lower $\delta^{13}C$ values than carbonate spherules forming at the sediment surface associated with photoautotrophy (Chen et al., 2022). Micrite in the Green Lake shoreline sediments precipitated from pore spaces in equilibrium with porewater $\delta^{13}C_{DIC}$ would contribute a lower-end member to the bulk carbonate $\delta^{13}C$ values.

Charophytes, the other major allochem at RIS, result from concurrent photosynthesis and carbonate precipitation. Charophyte algae mediate carbonate precipitation on their thalli to prevent local photosynthesis-inhibiting alkalinization and can contribute a significant mass to the lacustrine sediments of lakes they grow within (Pełechaty et al., 2013; Sand-Jensen et al., 2021). Photosynthetically driven calcification can occur rapidly, leading to isotopic disequilibrium with the surrounding water column, but this has only been observed in strongly evaporitic environments associated with decreased lake level and shoreline desiccation (Pentecost et al., 2006). The $\delta^{13}C_{carb}$ values of charophytes may be slightly ^{13}C-enriched or ^{13}C-depleted (~1–2‰) relative to water column DIC depending on the species, but still typically within the range of the $\delta^{13}C_{carb}$ values expected when in equilibrium with the local DIC (Pronin et al., 2016). The location where the RIS sediments were collected at Green Lake is not water-stressed, and therefore the charophyte calcite should record photosynthetically altered DIC compositions.

The charophyte grains provide unique evidence that both carbonate precipitation and dissolution likely occurred within the sediment. While charophyte thalli usually calcify, causing the preservation of a distinctive grain within the sediment, there were occurrences of excess calcite accumulated on the exterior of the charophyte grains within the sediment (Figure S5). Carbonate in excess of what is typically calcified suggests that carbonate continued precipitating on the charophyte grains after deposition. Furthermore, fragments of incomplete charophyte grains, including solution-enhanced pores and thinned walls, (Figures 4 and S5) suggest that dissolution after deposition likely caused the degradation of some charophyte grains. While it is possible that some fragmentation of charophyte grains could be caused by mechanical breakage, the wall thinning cannot be explained by mechanical breakage. If these features reflect *in situ* processes, the presence of both precipitation and dissolution features in both locations agrees with our finding that carbonate saturation state was spatially and seasonally variable.

The larger subhedral to euhedral calcite crystals that exist in the sediment separate from the intraclasts and oncoids (Figure 3f), which are a minor allochem at both sites, may be the product of water column whitings via photosynthetic phytoplankton (Stanton et al., 2022). DIC surrounding the cyanobacterial cell becomes locally ^{13}C-enriched during photosynthesis because it is energetically favorable for cyanobacterial cells to use $^{12}CO_2$ (Merz, 1992), thereby increasing localized $\delta^{13}C_{DIC}$ available for calcite precipitation. As a result, the $\delta^{13}C$ values of photosynthetic calcite crystals can be 4–5‰ higher than the average water column DIC (Havig et al., 2018; Thompson et al., 1990). We therefore interpret that whiting-generated calcite should contribute a high $\delta^{13}C$ end member to the bulk carbonate $\delta^{13}C$ values of our shoreline sediments and provide a record of water column primary productivity.

4.2 | Controls on porewater chemistry and carbon isotopes

4.2.1 | Porewater in disequilibrium with the water column

We evaluated the processes controlling porewater $\delta^{13}C_{DIC}$ values by comparing $\delta^{13}C_{DIC}$ at different locations in the lake (between BHE and RIS, and water column vs porewater) and by comparing the $\delta^{13}C$ of various carbon pools in the sediment (organic matter, DIC, and carbonate). The main factors controlling water column $\delta^{13}C_{DIC}$ are exchange with the atmosphere, $\delta^{13}C_{DIC}$ values of water inputs (rivers, groundwater, and surface runoff), and primary productivity (Leng & Marshall, 2004). During our 2020–2022 sampling, this combination of processes and sources yielded a relatively narrow range of $\delta^{13}C_{DIC}$ values of −6.9 to −8.7‰VPDB in the shallow (<1 m) waters. However, the significantly larger range of porewater $\delta^{13}C_{DIC}$ values across all seasons/cores (−10.2 to −19.5‰) did not overlap with the range observed from the shallow water column samples (Figure 6). We interpret the discordance in porewater versus lake water $\delta^{13}C_{DIC}$ values as evidence that the two DIC pools were controlled by different processes. Specifically, the porewaters were heavily affected by microbial carbon cycling even in the uppermost sediments.

In the pore fluids, organic matter remineralization and carbonate dissolution contribute to the concentration of porewater DIC and yield opposite effects on $\delta^{13}C_{DIC}$ values. In Green Lake, nearshore carbonate sediments had $\delta^{13}C$ values 3–4‰ higher than the water column DIC, and as expected, organic matter had lower $\delta^{13}C$ values than DIC and carbonate (Figure S8; Table S4). Microbial organic matter remineralization introduced ^{13}C depleted carbon in the form of dissolved CO_2 to the porewater DIC pool, thereby decreasing the porewater $\delta^{13}C_{DIC}$ value. In contrast, dissolution of ^{13}C-enriched carbonate increases porewater $\delta^{13}C_{DIC}$ values (Blättler et al., 2015). We interpret the ^{13}C-depleted porewater DIC in Green Lake as evidence that, in general, microbial organic matter remineralization had a stronger control on porewater DIC than carbonate dissolution in the shallow sediments. However, there were likely seasonal to interannual differences in the relative contribution of carbonate dissolution to the porewater DIC pool. For example, the Year 2 average porewater $\delta^{13}C_{DIC}$ values were higher than in Year 1, and the Year 2 Ω_{cal} values were lower than in Year 1. We interpret this as an increase in the contribution of carbonate dissolution, returning ^{13}C-enriched carbon to the DIC pool, in Year 2 relative to Year 1 (Figure 6). Aerobic oxidation of organic matter and carbonate dissolution are often coupled in sediments (Hu & Burdige, 2007) because aerobic oxidation of organic matter produces CO_2, which lowers Ω (Figure 9). However,

sediment oxygen microprofiling has shown that oxygen can be used up in the sediment by 5 cm, and can even be used up within the first few millimeters (e.g., Martin et al., 1998). Based on our 16S rRNA community data, we do not suspect aerobic respiration was a dominant metabolism in our sediments below 5 cm, and thus, did not yield a strong control on porewater $\delta^{13}C_{DIC}$ values. Below the 5 cm depth, microbes well known for sulfate reduction (an anerobic process), not aerobic respiration, were most abundant. Sulfate reduction can increase or decrease Ω_{cal}, depending on the organic molecule reduced and whether the sulfur product is oxidized (Section 4.3.1).

4.2.2 | Subsurface processes are influenced by seasonality in the water column

Seasonal processes in Green Lake also contribute to seasonal differentiation of sediment and porewater geochemistry. Episodic occurrence of annual late-spring to mid-summer whiting events cause seasonal differences in lake water ion concentrations and water column chemistry. Our porewater samples collected in spring 2021 (Year 1) yielded elevated alkalinity and $[Ca^{2+}]$ relative to fall 2020 and summer 2021. This indicates that the buildup of alkalinity and $[Ca^{2+}]$ in the water column preceding a whiting precipitation event also affects the sediment porewater. However, Ω_{cal} values and $[CO_3^{2-}]$ were not greater in the porewaters in spring 2021 than in fall 2020, due to lower average pH and higher average porewater [DIC] in spring 2021 (Figures 6 and S7). The elevated [DIC] may result from greater microbial organic matter remineralization, pointing to a microbial control on Ω_{cal} values independent of water column processes. In contrast, the alkalinity and $[Ca^{2+}]$ for our spring 2022 (Year 2) cores were not elevated relative to the other seasons, suggesting the spring whiting event may have been occurring during the spring Year 2 core sampling.

4.3 | Evidence for microbially driven authigenic carbonate precipitation in Green Lake

4.3.1 | Microbial effects on carbonate chemistry

Microbes living in sedimentary pore spaces can interact with carbonate geochemistry both passively by producing or consuming alkalinity and DIC, and actively by providing nucleation sites for $CaCO_3$ on negatively charged EPS (Braissant et al., 2007; Dupraz et al., 2009). Microbial organic matter remineralization alters both DIC and alkalinity, which ultimately can change pore space carbonate mineral saturation (Bergmann et al., 2013). The magnitude and direction of the caused change in alkalinity to the change in DIC ($\Delta ALK/\Delta DIC$) by a microbial metabolism will determine whether that metabolism will locally increase or decrease the Ω_{cal}. For most natural waters, the total ΔALK must exceed the total ΔDIC caused by a metabolism in order for Ω to increase. For example, aerobic respiration does not change alkalinity but increases DIC by producing CO_2 and can therefore decrease Ω_{cal} (Figure 9). Each candidate metabolism within the sediments at BHE and RIS has the potential to affect Ω_{cal}, which governs carbonate precipitation/dissolution in the pore spaces.

Calcite mineral saturation states for all but two cores decreased from the sediment–water interface to 10 cm depth (Figure 6). In the upper 5 cm, the dominant microbial class was Gammaproteobacteria, made up of families like Comamonadaceae (Figure 8), many of which are capable of aerobic heterotrophy (Willems, 2014). We attributed the decrease in saturation state in the uppermost sediment to aerobic oxidation of organic matter, which increases [DIC], decreases $\delta^{13}C_{DIC}$ values, lowers Ω_{cal} values, and has been observed to occur concurrently with carbonate dissolution (Hu & Burdige, 2007). However, cyanobacteria, mostly Synechococcales, were also present within all sediment samples at 5 cm depth, albeit at low abundance (≤3%), which is likely attributable to extraction bias as discussed in the results. Synechococcales are an order of coccoidal oxygenic photosynthetic cyanobacteria that have been previously reported as abundant in the Green Lake benthos and implicated in contributing to the formation of the bioherms (e.g., Thompson et al., 1990). Cyanobacterial pigments have been found on the surface of microbialites of Green Lake, further suggesting a photosynthetically active microbialite/sediment surface (Uveges et al., 2018). Although metabolisms cannot be directly inferred from the presence of DNA, prior microscopy-based research plus the presence of cyanobacterial sequences in the upper 5 cm of our sediment samples implies a photosynthetically active and aerobic environment at the sediment surface. Oxygenic photosynthesis, if occurring, would have the opposite effect on Ω_{cal} values versus aerobic respiration. The relatively high Ω_{cal} values at the sediment surface may indicate a net balance of photosynthesis vs. respiration in the upper portions of our sediment cores.

Below 5 cm, Ω_{cal} decreases and then stabilizes with depth in most samples, likely reflecting a shift in the net balance of microbial metabolisms away from photosynthesis. Ω_{cal} values were consistently >1 in all cores from fall 2020 through fall 2021 but dipped below 1 deeper than 15 cm in the remainder of the Year 2 cores. In all Year 1 cores, between 10 cm and ~20–25 cm depth, Ω_{cal} values increased or stayed relatively constant with depth.

We attribute the maintenance of calcite supersaturation in the anaerobic sediments in Year 1 to a high abundance of microbes likely capable of sulfate reduction such as Bathyarchaeia, Sva0485, Thermodesulfovibrionia and Desulfobaccia (Henry et al., 1994; Vuillemin et al., 2018; Zhou et al., 2018). In the BHE sediments, Bathyarchaeia are most abundant across all seasons below 5 cm (Figure 8). Members of Bathyarchaeia are capable of many anaerobic metabolisms, including sulfate and nitrate reduction, acetogenesis, and potentially anaerobic oxidation of methane (AOM) (Zhou et al., 2018). The second most abundant class in samples at BHE below 10 cm (Sva0485) is also capable of sulfate reduction (Concheri et al., 2017; Vuillemin et al., 2018). Sulfate concentration in the porewater at Green Lake is orders of magnitude higher than in most freshwater lakes (1.06–9.89 mmol), leading to an energetically favorable environment for sulfate to be the dominant electron acceptor. The

effect of the sulfate reduction metabolism on carbonate saturation is debated because it produces carbonate alkalinity in the form of HCO_3^- but also decreases alkalinity through the production of hydrogen sulfide (Bergmann et al., 2013; Gallagher et al., 2014; Meister, 2013):

$$C_{106}H_{175}O_{42} + 69SO_4^{2-} + 69H^+ \rightarrow 106HCO_3^- + 69H_2S$$

The above reaction leads to a net increase in alkalinity greater than the net increase in [DIC], resulting in an increase of Ω_{cal} (Figure 9). However, the true ΔALK/ΔDIC of sulfate reduction depends on the stoichiometry of the organic molecule or other terminal electron acceptors used by the microbe (Gallagher et al., 2014). While DNA is not directly indicative of metabolic activity, the presence of several organisms affiliated with sulfate-reducing metabolisms, high porewater sulfate concentrations, and dark sediment coloration are all consistent with the occurrence of sulfate reduction at depth in our sediments.

Given the persistence of $\Omega_{cal}>1$ in most core samples, we expect that *in situ* microbial sulfate reduction was a driver of authigenic carbonate precipitation in Green Lake sediments. Ω_{cal} was <1 below 15 cm depth for four cores (Figure 6), and $[Ca^{2+}]$ decreased with depth from the sediment surface to 20–25 cm depth in sediment for all cores. A lowered Ω_{cal} and decreased $[Ca^{2+}]$ is consistent with the precipitation of calcium carbonate minerals in situ. Alternatively, $\Omega_{cal}<1$ in some Green Lake porewater samples may suggest that sulfate reduction does not always produce conditions favoring carbonate precipitation.

At RIS, the sulfate reduction-affiliated clade Sva0485 was most abundant from 10 to 35 cm depth, but classes Aminicenantia and Dehalococcoidia were also common. Both consist of members that perform variations of anaerobic organoheterotrophic metabolisms and were also present (in lower abundance) at BHE. Their higher abundance at RIS, however, may be attributed to higher amounts of organic carbon in the surface sediments at RIS (Li et al., 2012; Salgado-Dávalos et al., 2021). Members of Aminicenantia and Dehalococcoidia are also capable of organohalide respiration (reduction of halogenated compounds using H_2 as an electron donor; Dong et al., 2019). Common organohalide respiration pathways, such as reductive dechlorination, are known as a common cause of groundwater acidification due to the release of hydrochloric acid (Futamata et al., 2007; Lacroix et al., 2014). The presence of the organohalide compounds typically respired by these taxa, such as trichloroethylene, perchloroethylene, and polychlorinated biphenyl have not been detected in FGL sediments but are common pollutants from agricultural pesticide and fertilizer usage. Green Lake is directly adjacent to a golf course, which can be a source of organohalide pollution from heavy fertilizer and pesticide use. If such metabolisms occur, the release of H^+ could cause a decrease in alkalinity (with no change to DIC, causing a decrease in Ω_{cal}; Figure 9) at a sub-millimeter scale where these taxa and organohalide compounds exist. "Microniches," or submillimeter-scale heterogeneity in geochemical variables like pH, have been observed in sediment and soil and can be caused by submillimeter heterogeneity in labile organic compounds (Cai et al., 2023; Stockdale et al., 2009). Further, simulations of reductive dechlorination in soils have been shown to cause the dissolution of minerals including calcite (Robinson et al., 2009). Thus, organohalide respiration and other acidifying metabolisms could contribute to the decrease in Ω_{cal} values with depth in the Year 2 cores and could account for the decrease in Ω_{cal} values at certain depths in the Year 1 cores.

At RIS, the percent abundance of bacteria from the clade Acetothermia increased from 0.2% of the sample at 15 cm to ~2% of the sample at 20 cm, and became the most abundant class by the deepest sample (35 cm) at RIS. The class Acetothermia is suggested to perform carbon fixation via an acetyl CoA pathway (Takami et al., 2012) using HCO_3^- and/or CO_3^{2-} as the carbon source (Korzhenkov et al., 2018). This form of chemoautotrophy — consumption of HCO_3^-/CO_3^{2-} — would decrease alkalinity and could be responsible for the observed decrease in Ω_{cal} values with increasing abundance of Acetothermia in RIS sediments (Figure 6). If decreasing Ω_{cal} resulted in carbonate dissolution, this could impact the bulk $\delta^{13}C_{carb}$ values. A pairwise Spearman-Rank correlation revealed a statistically significant correlation between the abundance of Acetothermia and $\delta^{13}C_{carb}$ in the Green Lake sediments, implying that Acetothermia may impact carbonate carbon isotopic compositions (Table S6).

As mentioned for sulfate reduction, the stoichiometry of the organic molecule being used, redox conditions, and speciation of metabolism products all affect the net ΔALK/ΔDIC and impact on the saturation state of carbonate minerals. To construct the vectors in Figure 9, we used an amended Redfield ratio for the stoichiometry following Bergmann et al. (2013). However, this organic molecule represents the average stoichiometry of phytoplankton in the pelagic ocean, not in sedimentary porewaters or lacustrine environments (Anderson, 1995). Without knowledge of the exact stoichiometry of the organic molecules being used in metabolism, the exact magnitude of the change in Ω_{cal} cannot be determined. Therefore, the arrows in Figure 9 should be viewed as estimates, not absolute values.

To further examine the interactions between microbial community and sediment geochemistry, we performed a Principal Coordinates Analysis (PCoA) on the 100 most abundant families present within the sediment at Green Lake (excluding water column data). Abundance of Bathyarchaeia (the most abundant family in the dataset, and the most abundant taxa in BHE >5 cm samples) and abundance of Sva0485 (second most abundant taxa in the dataset), both of which are sulfur-cycling anaerobes, appear to contribute strongly to the variance along axes 1 and 2, respectively (Figure 10a,b). When plotting axis 1 and 2 of the PCoA, nearly all samples plot along a linear path except most of the sediment top samples (5 cm samples). This distribution indicates that the 5 cm samples are most different from all deeper samples. Similarly, the 5 cm carbonate samples from different cores also have the highest variance and range in $\delta^{13}C_{carb}$ values out of all depths (Figure 10c; discussed further in Section 4.3.2). The $\delta^{18}O_{carb}$ values appear to vary along the linear trend of samples ≥10 cm in the PCoA, which could suggest

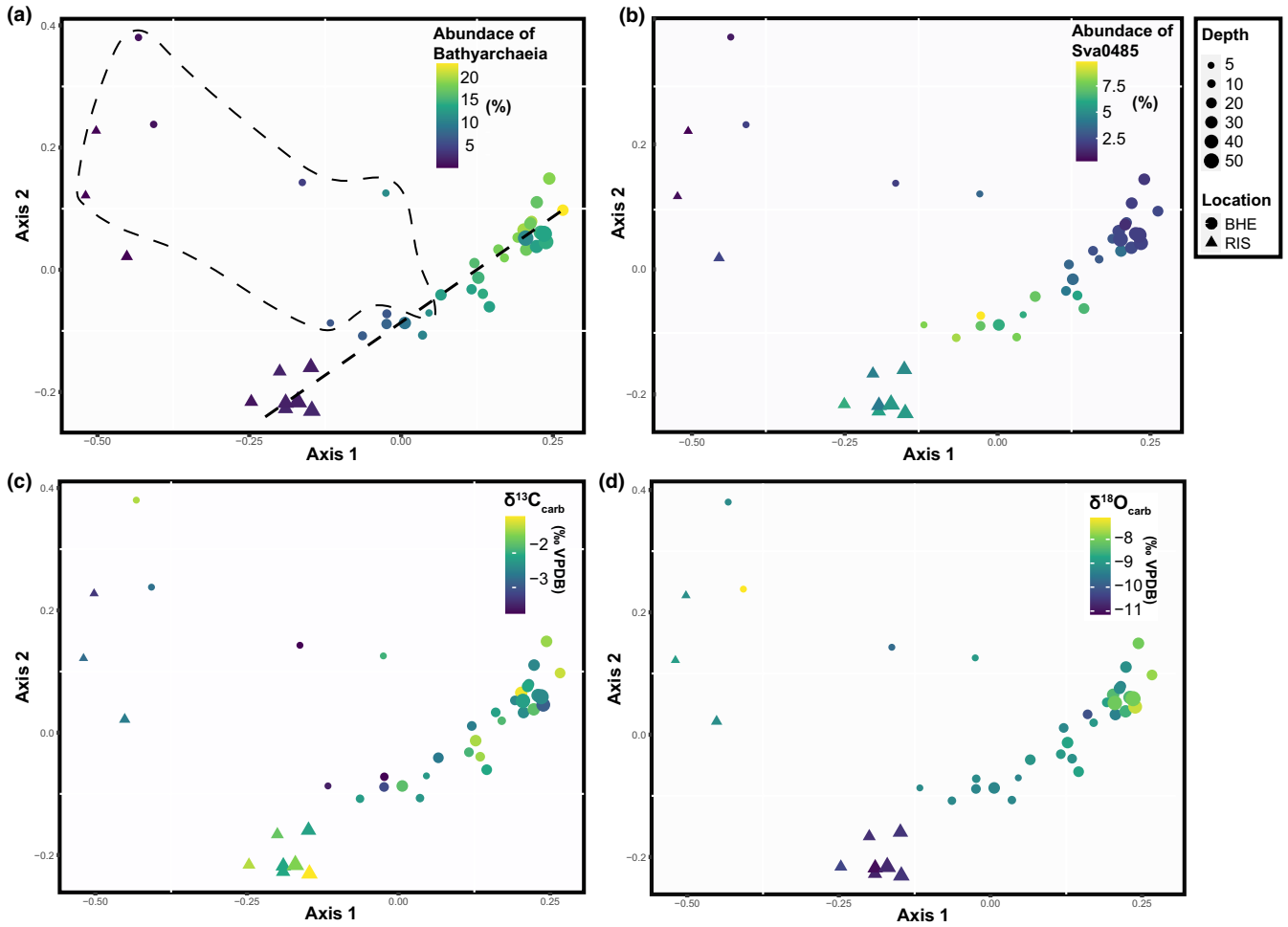

FIGURE 10 Principal Coordinate Analysis (PCoA) performed on 100 most abundant microbial family data (level 5) normalized to sample total sequence counts for sediment samples only, using package "Vegan" in R. Bray-Curtis distance matrix was used. Dotted lines in panel (a) used to demonstrate how data patterns differ between 5 cm and >5 cm samples. Each panel shows a different data variable (a and b) or attribute (c and d) represented by a color scale.

a potential co-variation with microbial taxa (Figure 10d). However, $\delta^{18}O_{carb}$ does not have a statistically significant variation with any of the 20 most abundant taxa (Table S6). Instead, the observed pattern is more likely due to location, a variable that causes differences in both $\delta^{18}O_{carb}$ (RIS is next to an inflow stream and BHE is not, impacting $\delta^{18}O$ of the source fluid) and microbial abundances (the microbial communities were somewhat different between the two locations, with Bathyarchaeia more abundant at BHE).

4.3.2 | Evidence for seasonal and spatial carbon isotope discontinuity

Carbonate sediment isotopic compositions varied laterally between and within sites, with depth, and through time. We observed differences in $\delta^{13}C$ values of carbonate sediment collected from the same depths in the same site but collected in different seasons. In fact, $\delta^{13}C_{carb}$ values were more similar (i.e. smaller sum of residuals) from the same depth between cores taken from the two different sites in one season (BHE and RIS cores, summer 2021) than when comparing $\delta^{13}C$ values of same depth samples taken in different seasons at a single site (BHE). Differences in downcore $\delta^{13}C_{carb}$ values from samples collected in similar locations but different seasons suggest that there may have been hyper-local differences in authigenic carbonate formation. Moreover, in spring 2022, we observed differences in $\delta^{13}C_{carb}$ at the same depths from two cores extracted on the same day only ~1 m apart from each other (Figure 6; Spring 2022a and Spring 2022b at BHE). Spatial heterogeneity of $\delta^{13}C_{carb}$ on a meter-scale necessitates that there are spatially varying controls on carbonate geochemistry at a <1 m scale. Here, we hypothesize that the seasonal and spatial differences observed in $\delta^{13}C_{carb}$ at the same depth horizons can be explained by both (1) spatial and seasonal variations in authigenic carbonate precipitation and dissolution, potentially caused by variation of microbial communities and (2) sediment reworking resulting in spatially varying proportions of the different allochems that record either photic zone or porewater processes.

We suggest that $\delta^{13}C_{carb}$ variability is strongly dependent on carbonate proto-facies. Although there were differences in the microbial communities observed between sites and seasons, the most

abundant classes remained the same, and thus, likely not the sole control on $\delta^{13}C_{carb}$ variability between cores. The variability in $\delta^{13}C_{carb}$ at a given depth was more pronounced at BHE where the dominant carbonate allochem is microbial intraclast than at RIS where the dominant allochems are carbonate mud and charophyte. Although there is a ~3‰ range in $\delta^{13}C_{carb}$ values downcore at RIS, between seasons, the $\delta^{13}C_{carb}$ values at a given depth horizon were very similar for the duration of our study. Thus, the sediment $\delta^{13}C_{carb}$ is relatively less laterally variable at the meter scale at RIS (Figure 6). The dominance of micrite and calcified charophytes at RIS suggests these allochems may record $\delta^{13}C_{carb}$ values that remain unaltered by microbial early diagenesis on timescales longer than 2 years.

The sediment at BHE is comprised of physical mixtures of thrombolite intraclasts, oncoids, and micrite, with some contribution of larger calcite crystals from whiting events, each likely contributing different end member $\delta^{13}C_{carb}$ values to the bulk carbonate signature. If the micrite is forming within the porewaters, potentially from in situ sulfate reduction, we would expect $\delta^{13}C_{carb}$ values to decrease with depth. The oncoids also become more micritic (less shrubby calcite) with depth, possibly pointing to micritization/*in situ* formation of these grains with depth.

As a result of authigenic micrite formation, we would expect to see $\delta^{13}C_{carb}$ values decrease with depth and negatively covary with Ω_{cal} values. We applied a simple linear mixing model to predict the mass fraction of authigenic carbonate precipitating at each depth based on the change in $\delta^{13}C_{carb}$ values between sampling time points. For example, the spring and summer 2021 $\delta^{13}C_{carb}$ values at 5 cm depth at BHE were −1.49‰ and −2.90‰, respectively. If we assume the authigenic carbonate is precipitating from the DIC of the porewater in summer 2021 ($\delta^{13}C_{DIC} = -14.00‰$), and an apparent fractionation, ε, between dissolved HCO_3^{2-} and solid $CaCO_3$ of +1.27‰ (Emrich et al., 1970), carbonate precipitating from this DIC pool should have a $\delta^{13}C_{carb}$ of −12.73‰. We can calculate the fraction of new or authigenic carbonate required to yield the summer 2021 5 cm sample using the spring 2021 composition as the primary endmember (−1.49‰), −12.73‰ as the secondary endmember, and the summer 2021 $\delta^{13}C_{carb}$ value as the resultant mixture (−2.90‰), in the following simple mixing model:

$$-1.48‰\,(f_{prim}) + -12.73‰\,(f_{auth}) = -2.90‰$$

$$f_{prim} + f_{auth} = 1$$

where f_{prim} is the fraction of carbonate precipitated or deposited at the sediment–water interface and authigenic carbonate formed prior to spring 2021 and f_{auth} is the fraction of authigenic carbonate formed between spring and summer 2021 sampling periods. Solving for f_{auth}, we find that an addition of 13% authigenic carbonate is required to change the bulk $\delta^{13}C_{carb}$ from −1.48‰ in the spring 2021 to −2.90‰ in summer 2021. Similar calculations could be performed for each depth for an estimate of the amount of authigenic precipitation occurring and/ or if there was instead net dissolution.

This trend of decreasing $\delta^{13}C_{carb}$ with depth is not observed in all cores. Furthermore, the range of $\delta^{13}C_{carb}$ values across all cores/seasons decreases with depth from 2.44‰ at 5 cm to 1.45‰ at 25 cm depth (Figures 6 and S9). However, the average of all cores' $\delta^{13}C_{carb}$ values do not decrease with depth (Figure S9) and do not correlate with Ω_{cal} values. We hypothesize that the reason that we do not observe a simple relationship between $\delta^{13}C_{carb}$ values and depth may result from either (1) different proportions of allochems or (2) that authigenic micrite is sediment-buffered, resulting in $\delta^{13}C_{carb}$ similar to primary carbonate. Lateral variability in relative amounts of allochems was observed (Figure S18). However, this mechanism cannot help to explain the reduction in $\delta^{13}C_{carb}$ variability with depth. The second mechanism, sediment buffered authigenesis, would suggest that authigenic micrite is precipitating from a DIC pool that is not in equilibrium with the porewaters but is instead directly impacted by carbonate dissolution. This style of early diagenesis could also help explain the decrease in $\delta^{13}C_{carb}$ range with depth. However, sediment-buffered early diagenesis of carbon isotopes typically only occurs in diffusion-dominated systems and/or when there is significantly less carbon in the pore space fluid than there is in the sediment, and is therefore unlikely here. Nonetheless, the overall decreased range in $\delta^{13}C_{carb}$ with depth suggests that early diagenesis may be homogenizing the preserved isotope values (Figure S9). This implies if spatial uniformity in stable isotope values is observed in facies dominated by microbialite clasts in the lacustrine rock record, early diagenetic overprinting may have altered the original values.

4.3.3 | Carbonate clumped isotope-derived temperatures record a facies bias

The temperatures derived from carbonate-clumped isotope measurements ($T(\Delta_{47})$) record the temperature of mineral formation if the carbonate forms in thermodynamic equilibrium with the precipitating fluid (Eiler, 2007). Therefore, if carbonate precipitates in the water column, it should record a water column temperature, whereas authigenic carbonate would record a porewater temperature. Water temperature at our shoreline sites ranged from 10.4 to 25.4°C, but $T(\Delta_{47})$ recorded by the upper 50 cm of sediment was restricted to $14.5^{+2.4}/_{-2.4}$ to $21.5^{+2.3}/_{-2.3}$°C at BHE and $12.2^{+2.9}/_{-2.8}$ to $14.9^{+2.3}/_{-2.2}$°C at RIS (Figure 5). The 5 cm samples at BHE yielded $T(\Delta_{47})$ values that reflected seasonal changes in lake water temperature. For example, the measured lake water temperature in fall 2020 (19.8°C) is within the uncertainty of the fall 2020 calculated $T(\Delta_{47})$ ($18.2^{+2.3}/_{-2.2}$°C). Although $T(\Delta_{47})$ of the spring 2021 BHE sample ($16.7^{+2.2}/_{-2.2}$°C) is not within the uncertainty of the measured lake water temperature (10.4°C) at the time of sampling, this was the lowest $T(\Delta_{47})$ measured in the BHE dataset. Similarly, summer 2021 measured lake water temperature (25.4°C) is not within the uncertainty of the calculated $T\Delta_{47}$ ($21.5^{+2.3}/_{-2.3}$°C), but both measured lake water temperature and $T\Delta_{47}$ are the highest out of all Year 1 BHE 5 cm samples. Similar to the mass balance argument for $\delta^{13}C$ homogenization, the significant seasonal differences in $T(\Delta_{47})$ at 5 cm suggest that there is enough new carbonate formation between seasons

to pull the physical mixture of new and "old" carbonate towards the temperature of new carbonate formation.

The seasonality of $T(\Delta_{47})$ in the uppermost sediments may suggest that carbonate production in the photic zone is abundant enough to contribute to a seasonal isotopic signal. Following the logic of the carbon isotope mixing model, we performed a non-linear mixing calculation to determine what mass fraction of newly forming carbonate would be required to change the Δ_{47} value at 5 cm from one season to the next (Defliese & Lohmann, 2015; Data S1 section 1.8). We considered a physical mixture of "primary" carbonate and carbonate formed between sampling timepoints that are in equilibrium with the temperature of shallow porewater at that season. For example, if we consider the spring 2021 BHE 5 cm Δ_{47} value (0.618‰) as the primary end member and calculate the second end-member Δ_{47} based on equilibrium with the summer 2021 porewater temperature (0.597‰), a mass fraction of 71% "new" carbonate is required to yield a final measured Δ_{47} of 0.603‰. This is much higher than the 13% of authigenic carbonate predicted by the $\delta^{13}C$ linear mixing model between the same two samples, and we lack petrographic evidence to suggest that over half of the carbonate in summer 2021 at 5 cm is newly formed.

The mixing calculation above assumes that the carbonate forming between seasons precipitates in isotopic equilibrium with the DIC pool. However, kinetics of DIC dehydration/dehydroxylation reactions have been shown to result in lower Δ_{47} values than predicted for thermodynamic equilibrium (e.g., Bajnai et al., 2020; Fiebig et al., 2021; Guo, 2020; Lu & Swart, 2023). CO_2 removal via photosynthesis can result in CO_2 dehydration/dehydroxylation, which would result in kinetic isotope effects that lower Δ_{47} values. If we apply the mass fractions of 13% new carbonate and 87% primary from the carbon isotope mass balance calculations, we calculate a Δ_{47} value of ~0.500‰ for the summer-forming carbonate at 5 cm, which supports our hypothesis of photosynthetically driven disequilibrium. Therefore, the range of Δ_{47} values captured at 5 cm is likely due to both a mass fraction of carbonate precipitation each season, potentially disequilibrated from the local DIC pool, and horizontal heterogeneity of sediment composition and source.

$T(\Delta_{47})$ generally converged downcore at BHE to approximately 18.5°C regardless of the sampling season, which represents the average temperature of the fall, spring, and summer seasons of the 2020–2021 sampling season. If this is due strictly to pore space carbonate precipitation, it could require up to 39% mass fraction of authigenic carbonate precipitation to achieve largest the change in Δ_{47} observed from 5 to 10 cm depth (summer 2021 core; Data S1 section 1.8). Instead, the convergence is likely due to a combination of both pore space precipitation at 10 cm and time averaging of the primary photic zone carbonate and authigenic carbonate previously formed between 0 and 10 cm depth. At 25 cm depth, however, one sample (fall 2020) records a colder temperature of 14.5°C. The colder temperature of the fall 2020 25 cm sample could result from a higher fraction of authigenic carbonate precipitation at porewater temperatures colder than the overlying water column, or disequilibrium porewater processes resulting in higher than expected Δ_{47} values associated with CO_2 hydration/hydroxylation (Bajnai et al., 2020; Guo, 2020).

At RIS, the recorded $T(\Delta_{47})$ of the carbonate material is consistently colder than the temperatures recorded at BHE, in addition to being colder than the overlying water temperature, even in the top 5 cm of sediment. The colder temperatures here could result from a spring-season bias, such that most of the carbonate material is derived from a whiting event happening in spring each year. However, whiting events extend until July, and there are no reports of whitings happening at different times in different portions of the lake. Instead, the colder temperatures could be the result of a facies-specific bias within the RIS core, with the majority of the carbonate material at RIS consisting of micrite and calcified charophyte fragments, not whiting crystals. Photosynthesis, performed by charophytes or microbes, and other microbial metabolisms may cause carbonate to form in disequilibrium with formation water due to processes affecting DIC interconversion, which can result in disequilibrium Δ_{47} values and inaccurate temperatures (Bajnai et al., 2020; Guo, 2020). Stable carbon isotopes have been used to show that charophytes can precipitate calcite in isotopic disequilibrium due to water stress, but disequilibrium in clumped isotopes has not yet been tested (Pentecost et al., 2006). Moreover, if the facies at RIS is indicative of a larger fraction of repreciptated carbonate material from the pore spaces, this may contribute to the observed colder $T(\Delta_{47})$. While most water column carbonate precipitation at Green Lake occurs in the late-spring to mid-summer (Brunskill, 1969) the average porewater temperatures are likely closer to the $T(\Delta_{47})$ recorded by RIS. A carbonate facies at RIS representative of a larger fraction of porewater precipitated carbonate, then, may create $T(\Delta_{47})$ values that reflect a yearly average porewater temperature, while the facies at BHE reflect grains recording $T(\Delta_{47})$ of mainly spring–summer season average temperatures during water column precipitation.

To address whether precipitation of carbonate from the pore spaces could be responsible for observed downcore temperature variability and between-site variability, we measured porewater temperatures during the spring 2022 sampling season (Figure 5). At BHE, the porewater temperatures are colder than the $T(\Delta_{47})$ recorded by the carbonate for all seasons, and, inversely, porewater temperatures are warmer than the $T(\Delta_{47})$ of the carbonates at RIS. The porewater temperatures, however, are variable at hourly, daily, and seasonal timescales, although the variability is dampened relative to the overlying water column. BHE porewater temperatures were measured in the morning, and RIS porewater temperature in the afternoon on the same day – over which time there was an increase in air temperature that also increased surface water and porewater temperatures. It is most likely that the carbonate $T(\Delta_{47})$ values do not result from a single precipitation event; rather, the $T(\Delta_{47})$ variability is likely from a combination of carbonate precipitating at water column temperatures, porewater temperatures, and carbonate precipitating in disequilibrium due to microbial carbon cycling processes.

4.4 | Implications for the lacustrine rock record

We have demonstrated that in the shoreline sediment in Green Lake, microbial carbon cycling as well as variable inputs of different allochems likely contribute to lateral variability of carbonate carbon, oxygen, and clumped isotope geochemistry. Time averaging of the 5 cm depth increments, which each integrate deposition on decadal to centennial timescales, mutes some of this variability. However, the lateral, meter-scale variability does not entirely disappear for $\delta^{13}C_{carb}$, and the isotope values can differ between entirely different locations in a lake despite the decrease in lateral variability in a single location ($\delta^{18}O_{carb}$, Δ_{47}).

These findings suggest that bulk carbonate from the lacustrine rock record, especially in locations that have shoreline microbial facies such as mat textures, stromatolites, or thrombolites, cannot be assumed to be formed from one singular process or record one single variable. Where possible, a facies-specific or even allochem-specific approach to carbonate geochemistry may help to resolve different processes occurring within the lake. For example, the microbial carbonate facies of the Laney Member of the Green River Formation have been described for more than 50 years (Sarg et al., 2013; Surdam & Stanley, 1979). Facies- and microfabric-specific carbon, oxygen, and clumped isotope analyses of the Laney Member in western Colorado allowed Ingalls et al. (2022) to reconstruct both lake paleohydrology and controls on the occurrences of the charismatic "giant" stromatolites. Furthermore, there are paleolake systems that primarily preserve shallow/shoreline carbonate with microbial carbonate facies, like Member B of the Sheep Pass Formation (Fouch, 1979; Winfrey, 1960). Our work demonstrates that facies/allochem-specific work of such systems may help untangle climatic drivers and global carbon cycle variations of the isotopic values from those caused by microbiology.

Sediment cores extracted in modern lakes for more recent paleoclimate studies are often taken in the deepest part of the lake, or in a transect from the center of the lake to the shoreline, like cores that have been used in Green Lake paleoclimate studies (Hilfinger IV et al., 2001; Kirby et al., 2002). However, given the permanent redox stratification of Green Lake and the implications of redox stratification on chemical sediments, our shoreline sediments are expected to be dissimilar to coeval lake bottom cores. Green Lake's anoxic lake bottom sediments preserve varves (Brunskill, 1969), which suggests the carbonate remains unaltered. Havig et al. (2018) found evidence for potential co-occurrence of microbial methanogenesis and sulfate reduction in the anoxic sediment, which would have opposing effects on carbonate saturation state. If these metabolisms occur at approximately equal rates, the overall impact on carbonate saturation would be negligible, supporting the idea that the deeper sediments are largely unaltered and preserve a water-column signal of hydrologic balance and primary productivity. It is likely that this extends to most carbonate-producing, sulfate-rich, meromictic lakes. However, lakes with different bedrock, water chemistry, and mixing regimes will resultingly have different sediment microbial communities, impacting carbonate geochemistry in different ways.

5 | CONCLUSIONS

Prior to this work, Green Lake had two described microbially mediated carbonate sources: (1) annual whitings driven by water column cyanobacterial blooms and (2) meter-scale shoreline thrombolites (Stanton et al., 2022; Thompson et al., 1997; Wilhelm & Hewson, 2012). Here, we demonstrated the possibility of a third undocumented source of microbially mediated carbonate in Green Lake: authigenic micrite, genetically linked to subsurface microbial carbon cycling. Authigenic carbonate precipitation in the shoreline sediments at Green Lake, in combination with spatially variable proportions of different allochems with different average $\delta^{13}C_{carb}$ values, help to explain seasonally variable $\delta^{13}C_{carb}$ values at the same depth horizons, and variability of preserved Δ_{47} derived temperatures in our sediments. The abundance of bacterial and archaeal classes capable of sulfate reduction in our sediment samples and high porewater sulfate concentrations indicates that microbial sulfate reduction pathways are likely in the sediments. *In situ* sulfate reduction in our sediments appears to have driven supersaturated Ω_{cal} in most samples where sediment was likely anoxic, potentially promoting authigenic carbonate precipitation. However, acidifying metabolisms like organohalide respiration pathways (reductive dehalogenation in some halide-rich and organic-rich samples) may counteract the carbonate-favoring effects of sulfate reduction.

Our data suggests that within Green Lake, carbonate formation is linked to microbial carbon cycling in the water column, at the sediment–water interface, and within the sediments, in addition to influence from charophyte algae. This challenges the notion that modern lacustrine carbonate sediments can be ascribed to simple water-column formation processes recording secular change in hydroclimate and productivity. Using an allochem/facies-specific lens when evaluating lacustrine carbonates can provide insight into where and how the carbonate in a sample formed, allowing for more accurate and nuanced interpretations of bulk lacustrine carbonate stable and clumped isotope signatures, and deep-time, biological processes and physicochemical parameters. To adequately constrain these processes and interpret the signatures they may leave in the lacustrine carbonate sedimentary record, we must continue to describe both the physicochemical and biologic processes involved in lacustrine carbonate precipitation in the modern and identify the implications for the stable isotope signatures preserved in the sedimentary and rock records.

ACKNOWLEDGMENTS

We thank Allie Wyman, Allie Baczynski, Laura Liermann, and Garrett Shepherd for technical assistance in geochemical and isotopic measurements and petrography at Penn State and Riley Foster for field assistance and 16s rRNA extractions. We thank Simon Davis for technical assistance for the Protium IBEX. Funding was provided by NSF EAR 1826850 to KS, ET, CF, and subaward to MI, funds from Penn State to MI, and a Geological Society of America Graduate Research Grant to HL.

CONFLICT OF INTEREST STATEMENT

There are no conflicts of interest to report for this research.

DATA AVAILABILITY STATEMENT

All raw and processed isotope data, dissolved ion data, petrographic images, and processed 16s rRNA data can be found in the Open Science Framework data repository accessible at osf.io/whx94. All sequence FASTQ files used for this study were deposited to the public National Center for Biotechnology Information (NCBI) Sequence Read Archive (SRA) database under BioProject PRJNA916981 BioSample accession numbers SAMN35677971–SAMN35678027 accessible at https://www.ncbi.nlm.nih.gov/bioproject/PRJNA916981.

ORCID

Hanna C. Leapaldt https://orcid.org/0009-0001-5615-6480
Carie M. Frantz https://orcid.org/0000-0003-2544-9245
Juliana Olsen-Valdez https://orcid.org/0009-0000-0092-9707
Kathryn E. Snell https://orcid.org/0000-0001-5373-7143
Elizabeth J. Trower https://orcid.org/0000-0001-9898-5589
Miquela Ingalls https://orcid.org/0000-0002-7451-2944

REFERENCES

Águila, B., Alcántara-Hernández, R. J., Montejano, G., López-Martínez, R., Falcón, L. I., & Becerra-Absalón, I. (2021). Cyanobacteria in microbialites of Alchichica Crater Lake: A polyphasic characterization. *European Journal of Phycology*, *56*(4), 428–443. https://doi.org/10.1080/09670262.2020.1853815

Anderson, L. A. (1995). On the hydrogen and oxygen content of marine phytoplankton. *Deep Sea Research Part I: Oceanographic Research Papers*, *42*(9), 1675–1680. https://doi.org/10.1016/0967-0637(95)00072-E

Anderson, N. T., Kelson, J. R., Kele, S., Daëron, M., Bonifacie, M., Horita, J., Mackey, T. J., John, C. M., Kluge, T., Petschnig, P., Jost, A. B., Huntington, K. W., Bernasconi, S. M., & Bergmann, K. D. (2021). A unified clumped isotope thermometer calibration (0.5–1,100°C) using carbonate-based standardization. *Geophysical Research Letters*, *48*(7), e2020GL092069. https://doi.org/10.1029/2020GL092069

Apprill, A., McNally, S., Parsons, R., & Weber, L. (2015). Minor revision to V4 region SSU rRNA 806R gene primer greatly increases detection of SAR11 bacterioplankton. *Aquatic Microbial Ecology*, *75*(2), 129–137. https://doi.org/10.3354/ame01753

Bajnai, D., Guo, W., Spötl, C., Coplen, T. B., Methner, K., Löffler, N., Krsnik, E., Gischler, E., Hansen, M., Henkel, D., Price, G. D., Raddatz, J., Scholz, D., & Fiebig, J. (2020). Dual clumped isotope thermometry resolves kinetic biases in carbonate formation temperatures. *Nature Communications*, *11*, 4005. https://doi.org/10.1038/s41467-020-17501-0

Bergmann, K. D., Grotzinger, J. P., & Fischer, W. W. (2013). Biological influences on seafloor carbonate precipitation. *PALAIOS*, *28*(2), 99–115. https://doi.org/10.2110/palo.2012.p12-088r

Blättler, C. L., Miller, N. R., & Higgins, J. A. (2015). Mg and Ca isotope signatures of authigenic dolomite in siliceous deep-sea sediments. *Earth and Planetary Science Letters*, *419*, 32–42. https://doi.org/10.1016/j.epsl.2015.03.006

Bolyen, E., Rideout, J. R., Dillon, M. R., Bokulich, N. A., Abnet, C. C., Al-Ghalith, G. A., Alexander, H., Alm, E. J., Arumugam, M., Asnicar, F., Bai, Y., Bisanz, J. E., Bittinger, K., Brejnrod, A., Brislawn, C. J., Brown, C. T., Callahan, B. J., Caraballo-Rodríguez, A. M., Chase, J., … Caporaso, J. G. (2019). Reproducible, interactive, scalable and extensible microbiome data science using QIIME 2. *Nature Biotechnology*, *37*(8), 852–857. https://doi.org/10.1038/s41587-019-0209-9

Braissant, O., Decho, A. W., Dupraz, C., Glunk, C., Przekop, K. M., & Visscher, P. T. (2007). Exopolymeric substances of sulfate-reducing bacteria: Interactions with calcium at alkaline pH and implication for formation of carbonate minerals. *Geobiology*, *5*(4), 401–411. https://doi.org/10.1111/j.1472-4669.2007.00117.x

Brunskill, G. J. (1969). Fayetteville Green Lake, New York. II. Precipitation and sedimentation of calcite in a Meromictic Lake with laminated sediments[1]. *Limnology and Oceanography*, *14*(6), 830–847. https://doi.org/10.4319/lo.1969.14.6.0830

Cai, L., Ding, S., Chen, M., Zhong, Z., Sun, Q., & Wang, Y. (2023). Visualizing biogeochemical heterogeneity in soils and sediments: A review of advanced micro-scale sampling and imaging methods. *Critical Reviews in Environmental Science and Technology*, *53*(12), 1229–1253. https://doi.org/10.1080/10643389.2022.2128239

Callahan, B. J., McMurdie, P. J., Rosen, M. J., Han, A. W., Johnson, A. J. A., & Holmes, S. P. (2016). DADA2: High-resolution sample inference from Illumina amplicon data. *Nature Methods*, *13*(7), 581–583. https://doi.org/10.1038/nmeth.3869

Chen, M., Conroy, J. L., Geyman, E. C., Sanford, R. A., Chee-Sanford, J. C., & Connor, L. M. (2022). Stable carbon isotope values of syndepositional carbonate spherules and micrite record spatial and temporal changes in photosynthesis intensity. *Geobiology*, *20*(5), 667–689. https://doi.org/10.1111/gbi.12509

Chu, X., Zhang, T., Zhang, Q., & Lyons, T. W. (2007). Sulfur and carbon isotope records from 1700 to 800Ma carbonates of the Jixian section, northern China: Implications for secular isotope variations in proterozoic seawater and relationships to global supercontinental events. *Geochimica et Cosmochimica Acta*, *71*(19), 4668–4692. https://doi.org/10.1016/j.gca.2007.07.017

Claypool, G. E., & Kaplan, I. R. (1974). The origin and distribution of methane in marine sediments. In I. R. Kaplan (Ed.), *Natural gases in marine sediments* (pp. 99–139). Springer US. https://doi.org/10.1007/978-1-4684-2757-8_8

Concheri, G., Stevanato, P., Zaccone, C., Shotyk, W., D'Orazio, V., Miano, T., Piffanelli, P., Rizzi, V., Ferrandi, C., & Squartini, A. (2017). Rapid peat accumulation favours the occurrence of both fen and bog microbial communities within a Mediterranean, free-floating peat Island. *Scientific Reports*, *7*(1), 8511. https://doi.org/10.1038/s41598-017-08662-y

Coplen, T. B. (2007). Calibration of the calcite–water oxygen-isotope geothermometer at devils hole, Nevada, a natural laboratory. *Geochimica et Cosmochimica Acta*, *71*(16), 3948–3957. https://doi.org/10.1016/j.gca.2007.05.028

Currie, B. S., Polissar, P. J., Rowley, D. B., Ingalls, M., Li, S., Olack, G., & Freeman, K. H. (2016). Multiproxy paleoaltimetry of the late Oligocene-Pliocene Oiyug Basin, southern Tibet. *American Journal of Science*, *316*(5), 401–436. https://doi.org/10.2475/05.2016.01

Daëron, M. (2021). Full propagation of analytical uncertainties in Δ47 measurements. *Geochemistry, Geophysics, Geosystems*, *22*(5), 1–19. https://doi.org/10.1029/2020GC009592

Dansgaard, W. (1964). Stable isotopes in precipitation. *Tellus*, *16*(4), 436–468. https://doi.org/10.3402/tellusa.v16i4.8993

Defliese, W. F., & Lohmann, K. C. (2015). Non-linear mixing effects on mass-47 CO2 clumped isotope thermometry: Patterns and implications. *Rapid Communications in Mass Spectrometry*, *29*(9), 901–909. https://doi.org/10.1002/rcm.7175

DeMott, L. M., Napieralski, S. A., Junium, C. K., Teece, M., & Scholz, C. A. (2020). Microbially influenced lacustrine carbonates: A comparison of late quaternary Lahontan tufa and modern thrombolite from Fayetteville green Lake, NY. *Geobiology*, *18*(1), 93–112. https://doi.org/10.1111/gbi.12367

Dong, X., Greening, C., Rattray, J. E., Chakraborty, A., Chuvochina, M., Mayumi, D., Dolfing, J., Li, C., Brooks, J. M., Bernard, B. B., Groves, R. A., Lewis, I. A., & Hubert, C. R. J. (2019). Metabolic potential of uncultured bacteria and archaea associated with petroleum seepage in deep-sea sediments. *Nature Communications*, *10*(1), 1816. https://doi.org/10.1038/s41467-019-09747-0

Dupraz, C., Reid, R. P., Braissant, O., Decho, A. W., Norman, R. S., & Visscher, P. T. (2009). Processes of carbonate precipitation in modern microbial mats. *Earth-Science Reviews*, *96*(3), 141–162. https://doi.org/10.1016/j.earscirev.2008.10.005

Eiler, J. M. (2007). "Clumped-isotope" geochemistry—The study of naturally-occurring, multiply-substituted isotopologues. *Earth and Planetary Science Letters*, *262*(3), 309–327. https://doi.org/10.1016/j.epsl.2007.08.020

Eisenlord, S. D., & Zak, D. R. (2010). Simulated atmospheric nitrogen deposition alters actinobacterial community composition in forest soils. *Soil Science Society of America Journal*, *74*(4), 1157–1166. https://doi.org/10.2136/sssaj2009.0240

Emrich, K., Ehhalt, D. H., & Vogel, J. C. (1970). Carbon isotope fractionation during the precipitation of calcium carbonate. *Earth and Planetary Science Letters*, *8*(5), 363–371. https://doi.org/10.1016/0012-821X(70)90109-3

Fiebig, J., Daëron, M., Bernecker, M., Guo, W., Schneider, G., Boch, R., Bernasconi, S. M., Jautzy, J., & Dietzel, M. (2021). Calibration of the dual clumped isotope thermometer for carbonates. *Geochimica et Cosmochimica Acta*, *312*, 235–256. https://doi.org/10.1016/j.gca.2021.07.012

Fouch, T. D. (1979). Character and paleogeographic distribution of upper cretaceous (?) and Paleogene nonmarine sedimentary rocks in east-central Nevada. In J. M. Armentrout, M. R. Cole, & H. TerBest, Jr. (Eds.), *Pacific coast paleogeography symposium*, *No. 3. Pacific Section* (pp. 97–111). Society of Economic Paleontologists and Minerologists.

Frantz, C., Gibby, C., Nilson, R., Stern, C. J., Nguyen, M., Ellsworth, C., Dolan, H., Sihapanya, A., Aeschlimann, J., & Baxter, B. K. (2023). Desiccation of ecosystem-critical microbialites in the shrinking Great Salt Lake, Utah (USA). *PLOS Water*, *2*(9), e0000100. https://doi.org/10.1371/journal.pwat.0000100

Freytet, P., & Verrecchia, E. P. (2002). Lacustrine and palustrine carbonate petrography: An overview. *Journal of Paleolimnology*, *27*(2), 221–237.

Futamata, H., Yoshida, N., Kurogi, T., Kaiya, S., & Hiraishi, A. (2007). Reductive dechlorination of chloroethenes by Dehalococcoides-containing cultures enriched from a polychlorinated-dioxin-contaminated microcosm. *The ISME Journal*, *1*(6), 471–479. https://doi.org/10.1038/ismej.2007.42

Gallagher, K. L., Dupraz, C., & Visscher, P. T. (2014). Two opposing effects of sulfate reduction on carbonate precipitation in normal marine, hypersaline, and alkaline environments: COMMENT. *Geology*, *42*(1), e313–e314. https://doi.org/10.1130/G34639C.1

Garcia-Pichel, F., López-Cortés, A., & Nübel, U. (2001). Phylogenetic and morphological diversity of cyanobacteria in soil desert crusts from the Colorado plateau. *Applied and Environmental Microbiology*, *67*(4), 1902–1910. https://doi.org/10.1128/AEM.67.4.1902-1910.2001

Gellatly, A. M., & Lyons, T. W. (2005). Trace sulfate in mid-Proterozoic carbonates and the sulfur isotope record of biospheric evolution. *Geochimica et Cosmochimica Acta*, *69*(15), 3813–3829. https://doi.org/10.1016/j.gca.2005.01.019

Guo, W. (2020). Kinetic clumped isotope fractionation in the DIC-H2O-CO2 system: Patterns, controls, and implications. *Geochimica et Cosmochimica Acta*, *268*, 230–257. https://doi.org/10.1016/j.gca.2019.07.055

Havig, J. R., Hamilton, T. L., McCormick, M., McClure, B., Sowers, T., Wegter, B., & Kump, L. R. (2018). Water column and sediment stable carbon isotope biogeochemistry of permanently redox-stratified Fayetteville Green Lake, New York, U.S.A. *Limnology and Oceanography*, *63*(2), 570–587. https://doi.org/10.1002/lno.10649

Henry, E. A., Devereux, R., Maki, J. S., Gilmour, C. C., Woese, C. R., Mandelco, L., Schauder, R., Remsen, C. C., & Mitchell, R. (1994). Characterization of a new thermophilic sulfate-reducing bacterium. *Archives of Microbiology*, *161*(1), 62–69. https://doi.org/10.1007/BF00248894

Hilfinger, M. F., IV, Mullins, H. T., Burnett, A., & Kirby, M. E. (2001). A 2500 year sediment record from Fayetteville Green Lake, New York: Evidence for anthropogenic impacts and historic isotope shift. *Journal of Paleolimnology*, *26*(3), 293–305. https://doi.org/10.1023/A:1017560300681

Hu, X., & Burdige, D. J. (2007). Enriched stable carbon isotopes in the pore waters of carbonate sediments dominated by seagrasses: Evidence for coupled carbonate dissolution and reprecipitation. *Geochimica et Cosmochimica Acta*, *71*(1), 129–144. https://doi.org/10.1016/j.gca.2006.08.043

Ingalls, M., Fetrow, A. C., Snell, K. E., Frantz, C. M., & Trower, E. J. (2022). Lake level controls the recurrence of giant stromatolite facies. *Sedimentology*, *69*(4), 1649–1674. https://doi.org/10.1111/sed.12967

Ingalls, M., Frantz, C. M., Snell, K. E., & Trower, E. J. (2020). Carbonate facies-specific stable isotope data record climate, hydrology, and microbial communities in Great Salt Lake, UT. *Geobiology*, *18*(5), 566–593. https://doi.org/10.1111/gbi.12386

Ingalls, M., Rowley, D. B., Currie, B. S., & Colman, A. S. (2020). Reconsidering the uplift history and peneplanation of the northern Lhasa Terrane, Tibet. *American Journal of Science*, *320*(6), 479–532. https://doi.org/10.2475/06.2020.01

Ingalls, M., Rowley, D., Olack, G., Currie, B., Li, S., Schmidt, J., Tremblay, M., Polissar, P., Shuster, D. L., Lin, D., & Colman, A. (2017). Paleocene to Pliocene low-latitude, high-elevation basins of southern Tibet: Implications for tectonic models of India-Asia collision, Cenozoic climate, and geochemical weathering. *GSA Bulletin*, *130*(1–2), 307–330. https://doi.org/10.1130/B31723.1

Kamennaya, N. A., Hu, P., & Jansson, C. (2020). Sedimentation of ballasted cells-free EPS in meromictic Fayetteville Green Lake. *Geobiology*, *18*(1), 80–92. https://doi.org/10.1111/gbi.12366

Katoh, K., Misawa, K., Kuma, K., & Miyata, T. (2002). MAFFT: A novel method for rapid multiple sequence alignment based on fast Fourier transform. *Nucleic Acids Research*, *30*(14), 3059–3066. https://doi.org/10.1093/nar/gkf436

Kim, S.-T., & O'Neil, J. R. (1997). Equilibrium and nonequilibrium oxygen isotope effects in synthetic carbonates. *Geochimica et Cosmochimica Acta*, *61*(16), 3461–3475. https://doi.org/10.1016/S0016-7037(97)00169-5

Kirby, M., Patterson, W., Mullins, H., & Burnett, A. (2002). Post-younger dryas climate interval linked to circumpolar vortex variability: Isotopic evidence from Fayetteville Green Lake, New York. *Climate Dynamics*, *19*(3), 321–330. https://doi.org/10.1007/s00382-002-0227-y

Kohn, M. J. (2010). Carbon isotope compositions of terrestrial C3 plants as indicators of (paleo)ecology and (paleo)climate. *Proceedings of the National Academy of Sciences*, *107*(46), 19691–19695. https://doi.org/10.1073/pnas.1004933107

Korzhenkov, A. A., Teplyuk, A. V., Lebedinsky, A. V., Khvashchevskaya, A. A., Kopylova, Y. G., Arakchaa, K. D., Golyshin, P. N., Lunev, E. A., Golyshina, O. V., Kublanov, I. V., Toshchakov, S. V., & Gavrilov, S. N. (2018). Members of the uncultured taxon OP1 ("Acetothermia") predominate in the microbial community of an alkaline hot Spring at East-Tuvinian Upland. *Microbiology*, *87*(6), 783–795. https://doi.org/10.1134/S0026261718060115

Lacroix, E., Brovelli, A., Holliger, C., & Barry, D. A. (2014). Control of groundwater pH during bioremediation: Improvement and validation of a geochemical model to assess the buffering potential of

ground silicate minerals. *Journal of Contaminant Hydrology*, *160*, 21–29. https://doi.org/10.1016/j.jconhyd.2014.01.006

Leng, M. J., & Marshall, J. D. (2004). Palaeoclimate interpretation of stable isotope data from lake sediment archives. *Quaternary Science Reviews*, *23*(7), 811–831. https://doi.org/10.1016/j.quascirev.2003.06.012

Li, D., Sharp, J. O., Saikaly, P. E., Ali, S., Alidina, M., Alarawi, M. S., Keller, S., Hoppe-Jones, C., & Drewes, J. E. (2012). Dissolved organic carbon influences microbial community composition and diversity in managed aquifer recharge systems. *Applied and Environmental Microbiology*, *78*(19), 6819–6828. https://doi.org/10.1128/AEM.01223-12

Li, H.-C., & Ku, T.-L. (1997). Δ13C–δ18C covariance as a paleohydrological indicator for closed-basin lakes. *Palaeogeography, Palaeoclimatology, Palaeoecology*, *133*(1), 69–80. https://doi.org/10.1016/S0031-0182(96)00153-8

Lu, C., & Swart, P. K. (2023). The application of dual clumped isotope thermometer (Δ47 and Δ48) to the understanding of dolomite formation. *Geology*, *52*(1), 56–60. https://doi.org/10.1130/G51576.1

Martin, P., Granina, L., Martens, K., & Goddeeris, B. (1998). Oxygen concentration profiles in sediments of two ancient lakes: Lake Baikal (Siberia, Russia) and Lake Malawi (East Africa). *Hydrobiologia*, *367*(1), 163–174. https://doi.org/10.1023/A:1003280101128

McCormack, J., & Kwiecien, O. (2021). Coeval primary and diagenetic carbonates in lacustrine sediments challenge palaeoclimate interpretations. *Scientific Reports*, *11*(1), 7935. https://doi.org/10.1038/s41598-021-86872-1

Meister, P. (2013). Two opposing effects of sulfate reduction on carbonate precipitation in normal marine, hypersaline, and alkaline environments. *Geology*, *41*(4), 499–502. https://doi.org/10.1130/G34185.1

Meister, P., Mckenzie, J. A., Vasconcelos, C., Bernasconi, S., Frank, M., Gutjahr, M., & Schrag, D. P. (2007). Dolomite formation in the dynamic deep biosphere: Results from the Peru margin. *Sedimentology*, *54*(5), 1007–1032. https://doi.org/10.1111/j.1365-3091.2007.00870.x

Merz, M. U. E. (1992). The biology of carbonate precipitation by cyanobacteria. *Facies*, *26*, 81–101.

Meyer, K. M., & Kump, L. R. (2008). Oceanic Euxinia in earth history: Causes and consequences. *Annual Review of Earth and Planetary Sciences*, *36*(1), 251–288. https://doi.org/10.1146/annurev.earth.36.031207.124256

Parada, A. E., Needham, D. M., & Fuhrman, J. A. (2016). Every base matters: Assessing small subunit rRNA primers for marine microbiomes with mock communities, time series and global field samples. *Environmental Microbiology*, *18*(5), 1403–1414. https://doi.org/10.1111/1462-2920.13023

Pedregosa, F., Varoquaux, G., Gramfort, A., Michel, V., Thirion, B., Grisel, O., Blondel, M., Prettenhofer, P., Weiss, R., Dubourg, V., Vanderplas, J., Passos, A., Cournapeau, D., Brucher, M., Perrot, M., & Duchesnay, É. (2011). Scikit-learn: Machine learning in python. *The Journal of Machine Learning Research*, *12*(null), 2825–2830.

Pełechaty, M., Pukacz, A., Apolinarska, K., Pełechata, A., & Siepak, M. (2013). The significance of Chara vegetation in the precipitation of lacustrine calcium carbonate. *Sedimentology*, *60*(4), 1017–1035. https://doi.org/10.1111/sed.12020

Pentecost, A., Andrews, J. E., Dennis, P. F., Marca-Bell, A., & Dennis, S. (2006). Charophyte growth in small temperate water bodies: Extreme isotopic disequilibrium and implications for the palaeoecology of shallow marl lakes. *Palaeogeography, Palaeoclimatology, Palaeoecology*, *240*(3), 389–404. https://doi.org/10.1016/j.palaeo.2006.02.008

Petryshyn, V. A., Lim, D., Laval, B. L., Brady, A., Slater, G., & Tripati, A. K. (2015). Reconstruction of limnology and microbialite formation conditions from carbonate clumped isotope thermometry. *Geobiology*, *13*(1), 53–67. https://doi.org/10.1111/gbi.12121

Pietzsch, R., Tedeschi, L. R., Oliveira, D. M., dos Anjos, C. W. D., Vazquez, J. C., & Figueiredo, M. F. (2020). Environmental conditions of deposition of the lower cretaceous lacustrine carbonates of the Barra Velha formation, Santos Basin (Brazil), based on stable carbon and oxygen isotopes: A continental record of pCO2 during the onset of the oceanic anoxic event 1a (OAE 1a) interval? *Chemical Geology*, *535*, 119457. https://doi.org/10.1016/j.chemgeo.2019.119457

Poage, M. A., & Chamberlain, C. P. (2001). Empirical relationships between elevation and the stable isotope composition of precipitation and surface waters: Considerations for studies of Paleoelevation change. *American Journal of Science*, *301*(1), 1–15. https://doi.org/10.2475/ajs.301.1.1

Pronin, E., Pełechaty, M., Apolinarska, K., Pukacz, A., & Frankowski, M. (2016). Sharp differences in the d13C values of organic matter and carbonate encrustations but not in ambient water DIC between two morphologically distinct charophytes. *Hydrobiologia*, *773*, 177–191. https://doi.org/10.1007/s10750-016-2698-6

Quast, C., Pruesse, E., Yilmaz, P., Gerken, J., Schweer, T., Yarza, P., Peplies, J., & Glöckner, F. O. (2013). The SILVA ribosomal RNA gene database project: Improved data processing and web-based tools. *Nucleic Acids Research*, *41*(D1), D590–D596. https://doi.org/10.1093/nar/gks1219

Robeson, M. S., II, O'Rourke, D. R., Kaehler, B. D., Ziemski, M., Dillon, M. R., Foster, J. T., & Bokulich, N. A. (2021). RESCRIPt: Reproducible sequence taxonomy reference database management. *PLoS Computational Biology*, *17*(11), e1009581. https://doi.org/10.1371/journal.pcbi.1009581

Robinson, C., Barry, D. A., McCarty, P. L., Gerhard, J. I., & Kouznetsova, I. (2009). pH control for enhanced reductive bioremediation of chlorinated solvent source zones. *Science of the Total Environment*, *407*(16), 4560–4573. https://doi.org/10.1016/j.scitotenv.2009.03.029

Roduit, N. (2022). Image analysis toolbox for measuring and quantifying components of high-definition images. Version 1.3.4. https://jmicrovision.github.io/

Romanek, C. S., Grossman, E. L., & Morse, J. W. (1992). Carbon isotopic fractionation in synthetic aragonite and calcite: Effects of temperature and precipitation rate. *Geochimica et Cosmochimica Acta*, *56*(1), 419–430. https://doi.org/10.1016/0016-7037(92)90142-6

Rowley, D. B. (2007). Stable isotope-based Paleoaltimetry: Theory and validation. *Reviews in Mineralogy and Geochemistry*, *66*(1), 23–52. https://doi.org/10.2138/rmg.2007.66.2

Rozanski, K., Araguás-Araguás, L., & Gonfiantini, R. (1993). Isotopic patterns in modern global precipitation. In P. K. Swart, K. C. Lohmann, J. Mckenzie, & S. Savin (Eds.), *Climate change in continental isotopic records* (Vol. *78*, pp. 1–36). American Geophysical Union.

Salgado-Dávalos, V., Osorio-Avilés, S., Kamaraj, S. K., Vega-Alvarado, L., Juárez, K., Silva-Martínez, S., & Alvarez-Gallegos, A. (2021). Sediment microbial fuel cell power boosted by natural chitin degradation and oxygen reduction Electrocatalysts. *CLEAN – Soil, Air, Water*, *49*(3), 2000465. https://doi.org/10.1002/clen.202000465

Sand-Jensen, K., Martinsen, K. T., Jakobsen, A. L., Sø, J. S., Madsen-Østerbye, M., Kjær, J. E., Kristensen, E., & Kragh, T. (2021). Large pools and fluxes of carbon, calcium and phosphorus in dense charophyte stands in ponds. *Science of the Total Environment*, *765*, 142792. https://doi.org/10.1016/j.scitotenv.2020.142792

Sarg, J. F., Suriamin, Tänavsuu-Milkeviciene, K., & Humphrey, J. D. (2013). Lithofacies, stable isotopic composition, and stratigraphic evolution of microbial and associated carbonates, Green River Formation (Eocene), Piceance Basin, Colorado. *AAPG Bulletin*, *97*(11), 1937–1966. https://doi.org/10.1306/07031312188

Stanton, C., Barnes, B. D., Kump, L. R., & Cosmidis, J. (2022). A re-examination of the mechanism of whiting events: A new role for diatoms in Fayetteville Green Lake (New York, USA). *Geobiology*, *21*(2), 210–228. https://doi.org/10.1111/gbi.12534

Steinman, B. A., & Abbott, M. B. (2013). Isotopic and hydrologic responses of small, closed lakes to climate variability: Hydroclimate reconstructions from lake sediment oxygen isotope records and mass balance models. *Geochimica et Cosmochimica Acta*, *105*, 342–359. https://doi.org/10.1016/j.gca.2012.11.027

Stockdale, A., Davison, W., & Zhang, H. (2009). Micro-scale biogeochemical heterogeneity in sediments: A review of available technology and observed evidence. *Earth-Science Reviews*, *92*(1), 81–97. https://doi.org/10.1016/j.earscirev.2008.11.003

Surdam, R. C., & Stanley, K. O. (1979). Lacustrine sedimentation during the culminating phase of Eocene Lake Gosiute, Wyoming (Green River Formation). *GSA Bulletin*, *90*(1), 93–110. https://doi.org/10.1130/0016-7606(1979)90<93:LSDTCP>2.0.CO;2

Takami, H., Noguchi, H., Takaki, Y., Uchiyama, I., Toyoda, A., Nishi, S., Chee, G.-J., Arai, W., Nunoura, T., Itoh, T., Hattori, M., & Takai, K. (2012). A deeply branching thermophilic bacterium with an ancient acetyl-CoA pathway dominates a subsurface ecosystem. *PLoS One*, *7*(1), e30559. https://doi.org/10.1371/journal.pone.0030559

Talbot, M. R. (1990). A review of the palaeohydrological interpretation of carbon and oxygen isotopic ratios in primary lacustrine carbonates. *Chemical Geology: Isotope Geoscience Section*, *80*(4), 261–279. https://doi.org/10.1016/0168-9622(90)90009-2

Thaler, C., Katz, A., Bonifacie, M., Ménez, B., & Ader, M. (2020). Oxygen isotope composition of waters recorded in carbonates in strong clumped and oxygen isotopic disequilibrium. *Biogeosciences*, *17*(7), 1731–1744. https://doi.org/10.5194/bg-17-1731-2020

Thompson, J. B., & Ferris, F. G. (1990). Cyanobacterial precipitation of gypsum, calcite, and magnesite from natural alkaline lake water. *Geology*, *18*(10), 995–998. https://doi.org/10.1130/0091-7613(1990)018<0995:CPOGCA>2.3.CO;2

Thompson, J. B., Ferris, F. G., & Smith, D. A. (1990). Geomicrobiology and sedimentology of the mixolimnion and chemocline in Fayetteville Green Lake, New York. *PALAIOS*, *5*(1), 52–75. https://doi.org/10.2307/3514996

Thompson, J. B., Schultze-Lam, S., Beveridge, T. J., & Des Marais, D. J. (1997). Whiting events: Biogenic origin due to the photosynthetic activity of cyanobacterial picoplankton. *Limnology and Oceanography*, *42*(1), 133–141. https://doi.org/10.4319/lo.1997.42.1.0133

Thompson, L. R., Sanders, J. G., McDonald, D., Amir, A., Ladau, J., Locey, K. J., Prill, R. J., Tripathi, A., Gibbons, S. M., Ackermann, G., Navas-Molina, J. A., Janssen, S., Kopylova, E., Vázquez-Baeza, Y., González, A., Morton, J. T., Mirarab, S., Zech Xu, Z., Jiang, L., … Earth Microbiome Project Consortium. (2017). A communal catalogue reveals earth's multiscale microbial diversity. *Nature*, *551*(7681), 457–463. https://doi.org/10.1038/nature24621

Uveges, B. T., Teece, M. A., Fulton, J. M., & Junium, C. K. (2018). Environmental controls on pigment distributions in the freshwater microbialites of Fayetteville green Lake. *Organic Geochemistry*, *125*, 165–176. https://doi.org/10.1016/j.orggeochem.2018.08.012

Vuillemin, A., Horn, F., Friese, A., Winkel, M., Alawi, M., Wagner, D., Henny, C., Orsi, W. D., Crowe, S. A., & Kallmeyer, J. (2018). Metabolic potential of microbial communities from ferruginous sediments. *Environmental Microbiology*, *20*(12), 4297–4313. https://doi.org/10.1111/1462-2920.14343

Walters, W., Hyde, E. R., Berg-Lyons, D., Ackermann, G., Humphrey, G., Parada, A., Gilbert, J. A., Jansson, J. K., Caporaso, J. G., Fuhrman, J. A., Apprill, A., & Knight, R. (2015). Improved bacterial 16S rRNA gene (V4 and V4-5) and fungal internal transcribed spacer marker gene primers for microbial community surveys. *MSystems*, *1*(1), e00009-15. https://doi.org/10.1128/mSystems.00009-15

Warton, D. I., Duursma, R. A., Falster, D. S., & Taskinen, S. (2012). Smatr 3– An R package for estimation and inference about allometric lines. *Methods in Ecology and Evolution*, *3*(2), 257–259. https://doi.org/10.1111/j.2041-210X.2011.00153.x

Wilhelm, M. B., & Hewson, I. (2012). Characterization of Thrombolitic bioherm cyanobacterial assemblages in a meromictic marl Lake (Fayetteville Green Lake, New York). *Geomicrobiology Journal*, *29*(8), 727–732. https://doi.org/10.1080/01490451.2011.619635

Willems, A. (2014). The family Comamonadaceae. In E. Rosenberg, E. F. DeLong, S. Lory, E. Stackebrandt, & F. Thompson (Eds.), *The prokaryotes: Alphaproteobacteria and Betaproteobacteria* (pp. 777–851). Springer. https://doi.org/10.1007/978-3-642-30197-1_238

Winfrey, W. M. (1960). Stratigraphy, correlation, and oil potential of the sheep pass formation, east-central Nevada. In *Intermountain Association of Petroleum Geologists Eleventh Annual Field Conference Proceedings* (pp. 126–133). Salt Lake City.

Yilmaz, P., Parfrey, L. W., Yarza, P., Gerken, J., Pruesse, E., Quast, C., Schweer, T., Peplies, J., Ludwig, W., & Glöckner, F. O. (2014). The SILVA and "All-species Living Tree Project (LTP)" taxonomic frameworks. *Nucleic Acids Research*, *42*(D1), D643–D648. https://doi.org/10.1093/nar/gkt1209

Zeebe, R. E., & Wolf-Gladrow, D. A. (2001). *CO_2 in seawater: Equilibrium, kinetics, isotopes*. Elsevier.

Zhou, Z., Pan, J., Wang, F., Gu, J.-D., & Li, M. (2018). Bathyarchaeota: Globally distributed metabolic generalists in anoxic environments. *FEMS Microbiology Reviews*, *42*(5), 639–655. https://doi.org/10.1093/femsre/fuy023

SUPPORTING INFORMATION

Additional supporting information can be found online in the Supporting Information section at the end of this article.

How to cite this article: Leapaldt, H. C., Frantz, C. M., Olsen-Valdez, J., Snell, K. E., Trower, E. J., & Ingalls, M. (2024). Primary to post-depositional microbial controls on the stable and clumped isotope record of shoreline sediments at Fayetteville Green Lake. *Geobiology*, *22*, e12609. https://doi.org/10.1111/gbi.12609